MAPBIOMAS

MapBiomas General "Handbook"

Algorithm Theoretical Basis Document (ATBD)

Annual nighttime radiance

MapBiomas Brazil -Collection 11
Nighttime Radiance — Collection 1, Version 1.0
Algorithm Theoretical Basis Document
Annual VIIRS DNB radiance, 2013–2025

Version 1

August, 2026

Table of Contents

Executive Summary

MapBiomas Brazil Nighttime Radiance Collection 1 is a national series of annual rasters describing upward nocturnal radiance observed by the Visible Infrared Imaging Radiometer Suite Day/Night Band (VIIRS DNB). The collection covers the territory of Brazil for each complete calendar year from 2013 to 2025. Its purpose is to provide a methodologically consistent view of the spatial distribution and temporal evolution of satellite-observed nighttime radiance for use in the MapBiomas platform and in subsequent scientific, planning and policy analyses.

The collection is derived exclusively from the daily NASA Black Marble VNP46A2 Collection 2 product. The primary measurement is the direct DNB_BRDF_Corrected_NTL band, expressed in nW cm^-2 sr^-1. The accompanying mandatory-quality, cloud-mask, snow, lunar-irradiance and retrieval-age bands belong to the same VNP46A2 product and are used only for observation screening, weighting and provenance. No gap-filled radiance, auxiliary thematic predictor, reconstructed radiance or interannual trend model contributes to the annual estimator.

Each annual map is calculated from daily observations using one processing configuration for all years. Nighttime observations are screened for cloud, shadow, cirrus, snow or ice, aurora, lunar eclipse, mandatory quality and lunar irradiance. Accepted positive radiances are converted to dimensionless natural-log space. A median-absolute-deviation rule limits the influence of gross residual departures. The retained values receive transparent reliability weights based on the VIIRS cloud-confidence and cloud-mask-quality fields. The weighted log mean, weighted log variance and Kish effective sample size are then calculated. The principal output, expected_radiance, is obtained with the lognormal mean back-transformation, which accounts for log-space dispersion rather than returning only the geometric mean.

The annual product contains 18 co-registered bands describing four complementary components: annual radiance magnitude, within-year distribution and dispersion, observation support and conditional model diagnostics. The complete band dictionary, including units and interpretation, is provided in Appendix A.

VNP46A2 is distributed on a 15-arc-second grid commonly described as nominal 500 m. For MapBiomas integration, Collection 1 is delivered on a 250 m output grid using nearest-neighbour allocation. The 250 m value describes the spacing and alignment of the distributed grid; it does not increase the native spatial information of the VIIRS source and is not a super-resolution result.

Collection 1 was additionally evaluated through an executed empirical validation using 192 fixed native-support locations distributed across six Brazilian stress-test domains and four radiance strata. The same locations were assessed in 2019, 2021 and 2024, yielding 576 point-years from

206,624 archived VNP46A2 point-day observations. The quality-weighted lognormal annual expectation closely reproduced the empirical weighted arithmetic expectation calculated from the same retained daily observations, with a median absolute discrepancy of 0.40% and a 90th percentile of 1.83%. The median observed coverage of the model-implied central 80% interval was 0.800. Temporal-dependence-aware validation further showed that moving-block bootstrap intervals were 1.124 times wider than the analytical conditional intervals on median. The complete validation design, quantitative results, sensitivity analyses and reproducibility records are provided in Supplementary Validation Report S1.

This is the first MapBiomas Brazil collection dedicated to annual nighttime radiance. The uniform 2013-2025 processing chain, explicit VIIRS-only input boundary, robust annual estimator and joint distribution of radiance and observation-support metrics establish the baseline for future versions. The collection webpage is available through https://brasil.mapbiomas.org/en/, and public processing code is distributed through the MapBiomas Brazil GitHub organization at https://github.com/mapbiomas-brazil.

1. Introduction

1.1. Scope and content of the document

This Algorithm Theoretical Basis Document describes how MapBiomas Brazil Nighttime Radiance Collection 1 was produced. It follows the general MapBiomas ATBD structure and documents the product objective, input data, theoretical basis, processing sequence, annual estimator, output bands, spatial grid, quality assessment, practical use, limitations and collection evolution.

Sections normally used to document supervised land-cover classification are adapted to a continuous radiometric product. The functional equivalents of a feature space, legend, classification algorithm and post-classification procedure are, respectively, the daily VIIRS measurement and quality variables, the continuous band dictionary, the annual statistical estimator and the export-grid and metadata procedures. Appendix A defines every output band; Appendix B records the Collection 1 parameter configuration; and Appendix C identifies the reproducibility metadata associated with each production run.

The report describes the production of annual maps only. Analyses of trends, change points, causal drivers, land-cover relationships, ecological effects or socioeconomic associations may use the collection as an input, but they are not part of the map-generation algorithm. Supplementary Validation Report S1 accompanies this ATBD and documents the executed empirical validation of the annual estimator and its implementation, including the fixed validation-location registry, mathematical validation tests, temporal-support assessment, uncertainty analysis, parameter sensitivity, component ablation, cross-product consistency and quantitative results.

1.2. Overview

MapBiomas Brazil Nighttime Radiance Collection 1 provides a national series of annual VIIRS DNB radiance products for 2013–2025. The release scope, scientific purpose and principal source are summarized above and specified technically in §2.1.2 and §3.2. MapBiomas Brazil Nighttime Radiance currently comprises its first collection:

- Collection 1, Version 1.0: 2013 through 2025 (released in August 2026).

Collection 1 establishes the methodological, data, output-band, and software baseline for the MapBiomas Brazil Nighttime Radiance series. One multi-band image is produced for each year, and the same observation-selection rules and estimator parameters are applied throughout the entire 2013–2025 period. The collection uses a single national processing configuration across all Brazilian biomes and regions, without region-specific parameterization.

Annual products are generated from direct daily VIIRS observations using predefined quality screening, robust log-space outlier control, graded reliability weighting and lognormal back-transformation. The complete observation rules and estimator are defined in §§3.3-3.5. No auxiliary thematic predictor contributes to the annual radiance estimate. The MapBiomas Brazil Nighttime Radiance Collection 1 products are the following:

- Annual expected nighttime radiance maps (expected_radiance), representing the quality-weighted lognormal annual expectation of upward nocturnal radiance in nW cm^{-2} sr^{-1} and constituting the principal radiance layer of the collection;
- Log-space location and dispersion layers, including weighted_mean_log_radiance, log_variance, and log_standard_deviation, which describe the weighted location and within-year dispersion of accepted nighttime-radiance observations;
- Model-based relative dispersion (lognormal_cv), providing the lognormal coefficient of variation associated with the annual radiance distribution;
- Empirical radiance-distribution layers, including median_radiance, p10_radiance, and p90_radiance, which provide robust and less model-dependent summaries of the retained daily radiance observations;
- Observation-support layers, including n_eff, the Kish effective sample size after weighting; n_candidate, the number of observations retained after VIIRS quality screening and before robust outlier screening; and n_inlier, the number of observations retained after median-absolute-deviation screening;
- Temporal-coverage and screening diagnostics, including candidate_fraction, valid_fraction, and outlier_fraction, describing, respectively, pre-screening temporal coverage, retained temporal coverage, and the proportion of candidate observations removed by the robust screening procedure;
- Observation-quality and provenance layers, including mean_reliability, which summarizes the mean reliability of candidate observations, and mean_retrieval_age_days, which records the mean VNP46A2 retrieval-age value;
- Conditional uncertainty layers, ci95_low and ci95_high, providing the lower and upper conditional 95% bounds around the model-based annual expected radiance;

- A standardized output grid for MapBiomas integration. The original VNP46A2 data are distributed on a 15-arc-second grid, commonly described as nominal 500 m. Collection 1 is delivered on a 250 m output grid using nearest-neighbour allocation to support alignment with MapBiomas products. The 250 m spacing refers to the distributed grid and does not increase the native spatial information of the VIIRS source or constitute a super-resolution product;
- Processing infrastructure and reproducibility resources, including the public Python workflow based on the Google Earth Engine Python API, processing scripts, parameter configuration, output-band definitions, metadata, dependency files, example commands, numerical and configuration tests, and reproducibility information associated with production runs.

Together, these components form one 18-band annual image for each complete calendar year. Data, documentation and code access are specified in §5.3. Detailed interpretation of the radiance, dispersion and support variables is provided in §§3.4, 3.5 and 6.1.

Unlike categorical land-use and land-cover products, MapBiomas Brazil Nighttime Radiance Collection 1 is a continuous radiometric product and therefore does not contain mapped classes, class IDs, or class-specific colours. The annual radiance values should preferably be interpreted together with their observation-support information.

Collection 1 is the first MapBiomas Brazil release dedicated specifically to annual nighttime radiance and therefore establishes the baseline for future versions of the product. Formal rules governing future methodological changes and reprocessing are defined in §5.2. Any such changes, including the reprocessing of previous years, will be explicitly versioned and documented to preserve the transparency and temporal traceability of the series.

1.3. Region of Interest

The region of interest is the territory of Brazil. A user-supplied Earth Engine FeatureCollection defines the national boundary for spatial filtering, clipping and export. The boundary does not contribute explanatory information to the estimator and does not modify daily radiance values.

The collection is national and is not parameterized separately by biome, ecoregion or administrative unit. The same observation model is applied in the Amazon, Atlantic Forest, Caatinga, Cerrado, Pampa and Pantanal, as well as in urban, rural, coastal and inland areas. Users may summarize the outputs by biome or administrative boundary after production, provided that the continuous radiance values and their spatial support are preserved.

1.4. Key Science Applications

Satellite observations at night provide information on the location, magnitude and temporal behaviour of upward artificial-light emissions. VIIRS DNB data have been used for urban and infrastructure studies, disaster assessment, economic analysis, energy-access research and environmental applications, while their broad spectral response and satellite observation geometry require careful interpretation (Levin et al., 2020).

Collection 1 supports:

- national and regional mapping of satellite-observed nighttime radiance;
- comparison of annual radiance patterns between 2013 and 2025;
- assessment of changes in the spatial distribution and magnitude of artificial light;
- identification of areas with stable or variable annual observation profiles;
- integration with MapBiomas analyses as a continuous explanatory or contextual layer; and
- selection of locations for independent field or high-resolution follow-up studies.

The mapped measurement is upward radiance received by the VIIRS DNB at the satellite. It is not a direct measurement of illuminance at ground level, human visual brightness, spectral composition or sky brightness. Those quantities require different instruments or an explicit observation model.

2. Overview and Background Information

2.1. Context and Key Information

This section addresses complementary contextual and technical information relevant to understanding the data sources, computational environment, and implementation used to produce MapBiomas Brazil Nighttime Radiance Collection 1.

2.1.1. MapBiomas Brazil Nighttime Radiance Collection

MapBiomas Brazil Nighttime Radiance Collection 1 is the first continuous nighttime-radiance component developed for integration with the MapBiomas Brazil framework. Its release scope and product components are defined in §1.2.

The general coordination of the collection is carried out by MapBiomas Brazil, with technical coordination by PLAN-B as a MapBiomas technical collaboration. The institutional authorship is attributed to the MapBiomas Brazil Nighttime Radiance Team.

Collection 1 uses one national processing configuration for the entire Brazilian territory. The spatial scope and absence of biome-, ecoregion- or region-specific parameterization are defined in §1.3. Consequently, differences among annual radiance maps are not generated by regional algorithms or thematic models.

The collection is designed as a continuous radiometric product rather than a categorical land-use and land-cover classification. Its principal measurement is satellite-observed upward nighttime radiance, accompanied by information on within-year dispersion, observation support, temporal coverage, reliability, and conditional uncertainty. These complementary layers are distributed together so that radiance magnitude can be interpreted in relation to the amount and quality of information supporting each annual estimate.

2.1.2. Remote Sensing Data

The remote sensing dataset used in MapBiomas Brazil Nighttime Radiance Collection 1 is derived from the Visible Infrared Imaging Radiometer Suite Day/Night Band (VIIRS DNB) onboard the Suomi National Polar-orbiting Partnership (Suomi NPP) platform. VIIRS DNB is a calibrated low-light imaging band designed to observe radiance under nighttime conditions. Compared with the earlier Defense Meteorological Satellite Program Operational Linescan System (DMSP-OLS) record, VIIRS provides improved radiometric calibration, dynamic range, and spatial detail for nighttime-light analysis (Elvidge et al., 2017).

Collection 1 uses the NASA Black Marble VNP46A2 Collection 2 product. NASA Black Marble processes VIIRS observations to generate analysis-ready nighttime-light products incorporating atmospheric, terrain, lunar-BRDF, thermal, and stray-light corrections. VNP46A2 is a daily Level-3 product on the nominal 500 m source grid. It contains direct and gap-filled BRDF-corrected nighttime-light radiance bands together with cloud, snow, lunar, quality, and retrieval-age information (Román et al., 2018; NASA VIIRS Land SIPS, 2024).

The principal radiometric input is the direct DNB_BRDF_Corrected_NTL band, expressed in nW cm^{-2} sr^{-1}. The gap-filled band is excluded from the primary estimator; the resulting annual product is therefore based only on available direct observations satisfying the eligibility criteria specified in §3.3.

Additional source-product variables are used only for observation eligibility, reliability weighting and provenance. Their exact band names and roles are listed in §3.2. No auxiliary thematic dataset contributes to the primary annual estimator.

2.1.3. Google Earth Engine and MapBiomas Computer Applications

Processing of MapBiomas Brazil Nighttime Radiance Collection 1 is based on Google Earth Engine cloud-computing infrastructure. Earth Engine provides access to the daily NASA VNP46A2 archive and performs the pixelwise processing and annual statistical reductions on the server, while the client-side implementation defines the annual images, processing parameters, metadata, and export tasks.

The public implementation is written in Python and uses the Google Earth Engine Python API. The code contains no credentials, user-account information, Google Cloud project identifiers, private Earth Engine asset identifiers, or local file paths. Before execution, the user provides an Earth Engine-enabled Google Cloud project, a boundary FeatureCollection defining Brazil, and an Earth Engine asset folder or Google Drive destination for the outputs. Required configuration fields are documented in the processing script and README.

The Collection 1 software implementation provides:

- command-line configuration of processing years, observation-quality thresholds, reliability weights, and output-grid parameters;
- annual export to Earth Engine assets, Google Drive, or both;

- optional use of an exact affine transformation to reproduce the canonical MapBiomas output-grid alignment;
- a dry-run mode that constructs the annual products and verifies the expected output-band structure without initiating exports;
- optional monitoring of Earth Engine processing tasks with explicit reporting of failures;
- generation of a public JSON run manifest containing reproducibility information while omitting project, asset, task, credential, and local-path identifiers; and
- local numerical and configuration tests that can be executed without Earth Engine credentials.

The same parameter object is applied to all years selected within a production run. Release-level parameter, schema, grid and provenance requirements are specified in §3.7 and Appendix C. Each calendar year is processed and exported separately to support task management and selective rerunning. The operational implications are discussed in §6.2.

2.2. Historical Perspective and Existing Products

Satellite-based observation of nighttime lights predates the VIIRS era and has long been used to characterize the spatial distribution and temporal evolution of human-generated light emissions. Earlier nighttime-light records were produced from the Defense Meteorological Satellite Program Operational Linescan System (DMSP-OLS). The introduction of the Visible Infrared Imaging Radiometer Suite Day/Night Band (VIIRS DNB) onboard the Suomi National Polar-orbiting Partnership platform represented an important advance for nighttime-light remote sensing, providing improved radiometric calibration, dynamic range, and spatial detail compared with the earlier DMSP-OLS record (Elvidge et al., 2017).

NASA Black Marble extended the analytical value of VIIRS by providing corrected, analysis-ready daily and temporal-composite products. Collection 1 uses the direct daily corrected radiance described in §2.1.2 rather than the gap-filled radiance.

Several operational and research products provide important context for annual VIIRS compositing. These products differ in their observation-screening criteria, temporal aggregation procedures, radiance thresholds, treatment of snow and viewing geometry, and statistical estimands. Consequently, different annual nighttime-light products should be regarded as complementary representations of VIIRS observations rather than interchangeable estimates of a single error-free quantity.

2.2.1. Earth Observation Group VIIRS Nighttime-Light Products

The Earth Observation Group (EOG) produces cleaned monthly and annual VIIRS nighttime-light products based on cloud-free average radiance and additional screening designed to reduce the influence of background signals and ephemeral light sources (Elvidge et al., 2017; Elvidge et al., 2021). These products constitute an important operational global record of VIIRS-observed nighttime radiance and are widely used as reference layers in scientific and applied studies.

The annual EOG VIIRS nighttime-light product is also an appropriate external comparison dataset for MapBiomas Brazil Nighttime Radiance Collection 1 during overlapping years. However, it should not be interpreted as error-free reference truth because its screening procedures, temporal estimand, radiance thresholds, and compositing approach differ from those adopted in Collection 1. Comparisons between products therefore require attention to methodological differences rather than interpretation solely in terms of absolute agreement or disagreement.

2.2.2. NASA Black Marble Temporal Composite Products

In addition to the daily VNP46A2 product used as the source dataset for Collection 1, NASA Black Marble provides temporal composite products derived from VIIRS observations. VNP46A3 and VNP46A4 provide monthly and annual nighttime-light composites, respectively, together with information such as observation counts, standard deviation, and quality indicators. These products also incorporate stratification related to factors such as viewing angle and snow conditions (Wang et al., 2022).

NASA VNP46A4 Collection 2 represents an especially relevant external comparison layer for annual MapBiomas products. Nevertheless, differences between the two products are expected because NASA temporal composites apply their own observation-screening and arithmetic-averaging procedures, whereas MapBiomas Collection 1 uses robust log-space screening, graded observation reliability, effective-sample-size estimation, and a lognormal expected-radiance estimator. External comparison therefore requires harmonization of the harmonization requirements specified in §4.2 before quantitative metrics are calculated.

The choice of temporal compositing strategy is particularly important for nighttime-light data. The duration and composition of the temporal window can affect valid-data coverage, estimated radiance magnitude, and the suitability of the resulting composite for different applications (Zheng et al., 2022). In addition, daily VIIRS radiance spans several orders of magnitude and exhibits brightness-dependent variability, which supports the use of log-space characterization when comparing locations with very different radiance levels (Small, 2021).

2.2.3. MapBiomas Brazil nighttime Radiance Collection 1

MapBiomas Brazil Nighttime Radiance Collection 1 complements existing global VIIRS products by providing a national and reproducible annual processing chain specifically designed for integration with the MapBiomas framework. Rather than distributing only a single annual mean-radiance layer, Collection 1 retains radiance intensity, within-year dispersion, empirical distribution, observation support, temporal coverage, and conditional uncertainty as complementary components of the annual product. Collection 1 differs from conventional arithmetic compositing by combining robust log-space screening, graded observation-quality weighting, effective-sample-size estimation and lognormal back-transformation. The complete estimator is defined in §§3.3–3.5.

This structure allows Collection 1 to separate three components that are frequently combined or omitted in annual nighttime-light products: radiance magnitude, within-year temporal dispersion, and observation support. As a result, an annual radiance estimate can be interpreted together with information on how variable the underlying observations were and how much effective temporal information contributed to the estimate. Empirical validation confirms that this additional distributional structure is obtained without materially altering the annual radiance magnitude relative to the direct weighted arithmetic expectation: across 576 point-years, the median absolute difference was 0.40% and the 90th percentile was 1.83%. The purpose of the lognormal formulation is therefore distribution-aware annual representation rather than forecasting. It retains the central log-radiance, within-year multiplicative dispersion and effective temporal support as distinct quantities, whereas a single arithmetic annual mean collapses these properties into one value.

Collection 1 applies the same observation model and parameter configuration independently to every complete calendar year from 2013 to 2025. Annual images are not used to estimate adjacent years, and therefore the series contains no temporal smoothing between preceding and subsequent annual products. This standardization is intended to improve temporal comparability while retaining the annual observation-support information required to identify differences caused by variation in the number, timing, or geometry of valid observations.

MapBiomas Brazil Nighttime Radiance Collection 1 should therefore be considered complementary to EOG and NASA Black Marble annual composites rather than a replacement for them. Differences among these products reflect not only measurement variability but also explicit methodological choices concerning observation selection, robust screening, weighting, statistical estimation, temporal support, and output definitions. Comparative analyses should consequently examine both radiance values and the methodological characteristics of the products being compared.

The methods, processing workflow, and supporting code for Collection 1 are designed for public and reproducible implementation. MapBiomas Brazil information, collections, and download guidance are available through the MapBiomas Brazil platform, while the public Python workflow is distributed through the MapBiomas Brazil GitHub organization together with the processing script, documentation, dependency files, example commands, and tests.

3. Methodological Description

3.1. Overall Workflow

The processing chain contains six stages:

1. select daily VNP46A2 images for Brazil and one complete calendar year;
2. decode internal VIIRS quality information and mask unsuitable observations;
3. transform accepted positive radiance to dimensionless log space;
4. identify robust inliers with a median-absolute-deviation rule;
5. estimate weighted lognormal parameters and observation-support metrics; and
6. assemble, clip, document and export the annual multi-band image.

The same stages and parameters are applied separately to each year from 2013 through 2025. The annual images are not used to estimate each other; therefore a value for one year is not smoothed with preceding or subsequent years (Figure 1).

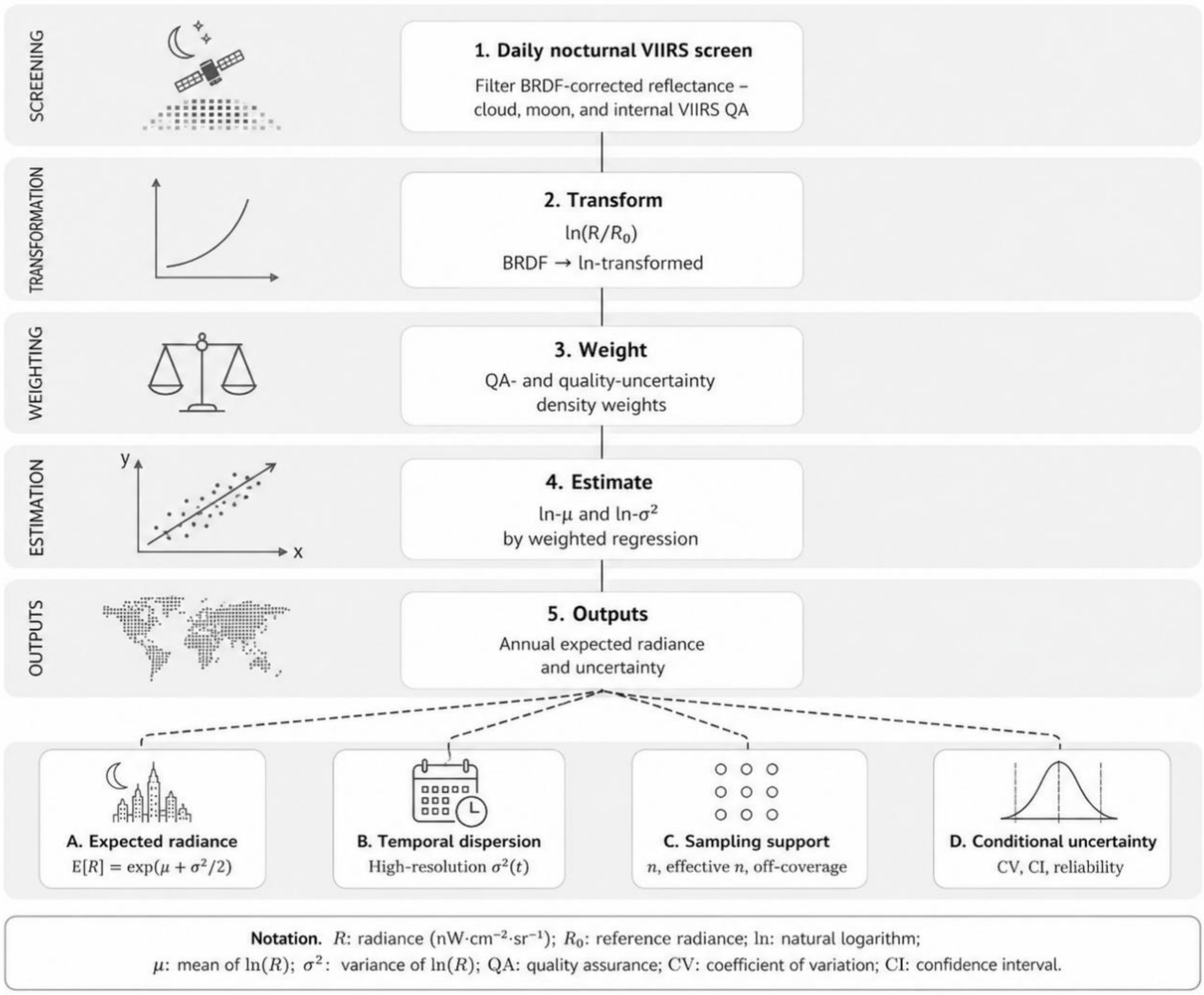

Figure 1. VIIRS-only production chain. Direct VNP46A2 radiance is screened and weighted using internal VIIRS quality information.

3.2. Input Data

The source collection is NASA/VIIRS/002/VNP46A2 in Google Earth Engine. The official Earth Engine catalogue describes the spatial grid, temporal cadence, band names and bit fields used by the implementation (Google Earth Engine, 2026a). The scientific product is NASA VIIRS/NPP Gap-Filled Lunar BRDF-Adjusted Nighttime Lights Daily L3 Global 15 arc-second Linear Lat Lon Grid, Collection 2, DOI 10.5067/VIIRS/VNP46A2.002 (NASA VIIRS Land SIPS, 2024b).

Source band	Role in Collection 1	Unit or encoding
DNB_BRDF_Corrected_NTL	Direct daily radiance used by the annual estimator	nW cm^-2 sr^-1
Mandatory_Quality_Flag	Restricts input to high-quality main-algorithm retrievals	Integer category
QF_Cloud_Mask	Provides night, surface, cloud-mask quality, cloud confidence, shadow, cirrus, snow or ice, aurora and lunar-eclipse flags	Packed bit field
Snow_Flag	Excludes snow-covered observations	Integer flag
DNB_Lunar_Irradiance	Applies the Collection 1 lunar-irradiance threshold	Product unit
Latest_High_Quality_Retrieval	Describes retrieval age in an output support metric	Days

The Gap_Filled_DNB_BRDF_Corrected_NTL band is not used in the primary estimator. The only non-VIIRS spatial input is the Brazil boundary, which is used for filtering, clipping and export.

3.3. Observation Variables and Quality Screening

The product does not use a conventional classification feature space. Its observation space consists of direct radiance and the internal VNP46A2 variables needed to determine whether and with what reliability that radiance enters the annual estimator.

An observation is accepted as an annual-composite candidate when all of the following conditions are satisfied:

Screening element	Collection 1 rule
Day/night flag	Night (QF_Cloud_Mask bit 0 equals 0)
Cloud-mask quality	Bits 4-5 are at least 1

Screening element	Collection 1 rule
Cloud confidence	Bits 6-7 are 0 or 1: confident clear or probably clear
Cloud shadow	Bit 8 equals 0
Cirrus	Bit 9 equals 0
Snow or ice surface	Bit 10 equals 0
Aurora	Bit 12 equals 0
Lunar eclipse	Bit 13 equals 0
Product snow flag	Snow_Flag equals 0
Mandatory quality	Mandatory_Quality_Flag equals 0
Lunar irradiance	Less than 30
Direct radiance	Greater than 0.10 nW cm^-2 sr^-1

The mandatory-quality rule follows the Collection 2 user guide, where value 0 identifies the high-quality main-algorithm retrieval and other values identify reduced-quality or exceptional retrieval conditions (NASA VIIRS Land SIPS, 2024a). The explicit aurora and lunar-eclipse checks provide an additional direct reading of the packed cloud-mask field. The positive radiance floor makes the logarithmic transformation numerically defined; it is a processing parameter and not a declared sensor-detection threshold.

Candidate observations receive a reliability score q_i. Confident-clear observations receive 1.00 and probably-clear observations receive 0.70. Medium or high cloud-mask quality receives 1.00 and low cloud-mask quality receives 0.80. The two components are multiplied. Because mandatory quality 0 is required before weighting, mandatory quality does not add a second graded multiplier.

3.4. Continuous Product Definition

The continuous product concept introduced in §§1.2 and 2.1.1 is implemented through the band dictionary in Appendix A. The equivalent of the legend is the continuous band dictionary in Appendix A. Its principal variable is annual expected radiance in nW cm^-2 sr^-1. The remaining bands describe log-space location and dispersion, empirical radiance distribution, effective observation support, temporal coverage and conditional uncertainty.

Visual colour ramps may be selected by the MapBiomas portal for communication, but colours do not define classes or thresholds. Analytical use should retain the native numerical values and units. The band name, data type, unit, nodata rule and interpretation are stored with the product metadata.

3.5. Annual Composite Estimation

For each output location and year, let R_i be the accepted direct daily radiance for observation i. The complete estimator is applied independently at every location. The positive radiance is first expressed as a dimensionless natural logarithm:

$$x_i = ln(R_i / R_0), \text{ with } R_0 = 1 \text{ nW cm^-2 sr^-1.}$$

The reference radiance $R0$ ensures that the logarithm operates on a dimensionless ratio. The transformation also reduces the influence of the multi-order-of-magnitude radiance range documented for VIIRS nighttime observations (Small, 2021). The median m and median absolute deviation MAD are calculated from candidate x_i values. The robust scale is max(1.4826 MAD, 10^{-6}), and the inlier indicator is:

$$I_i = 1 \text{ when } |x_i - m| \leq 3.5 \max(1.4826\ MAD, 10^{-6}), \text{ and 0 otherwise.}$$

The median absolute deviation provides a robust scale estimate with limited sensitivity to isolated extremes (Rousseeuw and Croux, 1993). The rejected proportion is retained in outlier_fraction. Reliability is converted to a nominal log-space uncertainty and effective weight:

$$u\_i = 0.03 + 0.30(1 - q_i);\ w\_i = I_i\, q_i / (1 + u_i{}^2).$$

The constants are fixed Collection 1 algorithm parameters. They provide a bounded, transparent reliability penalty; they are not a sensor-level inverse-variance calibration. The weighted mean log-radiance and Kish effective sample size are:

$$\mu w = \Sigma_i(w\_i\, x_i) / \Sigma_i(w\_i);\ n\_eff = [\Sigma_i(w\_i)]\text{^}2 / \Sigma_i(w\_i\text{^}2).$$

n_{eff} equals the retained observation count when all weights are equal and decreases when a small number of observations carry most of the total weight (Kish, 1965). The biased weighted second central moment is corrected using the effective sample size:

$$v\_b = \Sigma_i[w\_i(x_i - \mu w)\text{^}2] / \Sigma_i(w\_i);\ s_v{}^2 = v\_b\ n\_eff / (n\_eff - 1).$$

The variance is defined when n_{eff} is greater than 1. The public implementation requires n_{eff} of at least 2.0 before exporting the principal expected-radiance and conditional-interval values. $log_{variance}$ stores s_w^2, whereas $log_{standard\_deviation}$ stores its square root. If the accepted log-radiance profile is represented by a normal distribution, radiance follows a lognormal model and its expectation differs from the exponentiated log mean (Aitchison and Brown, 1957). The principal annual estimator is:

$$expected\_radiance = R_0 \, exp(\mu w + s_v{}^2 / 2).$$

Because the annual estimator is formulated in log space, the back-transformation to radiance depends not only on the weighted mean log-radiance but also on its dispersion. As log-space variance increases, the expected radiance increasingly differs from the simple exponentiation of the log mean, while relative variability also increases. These theoretical relationships are illustrated in Figure 2.

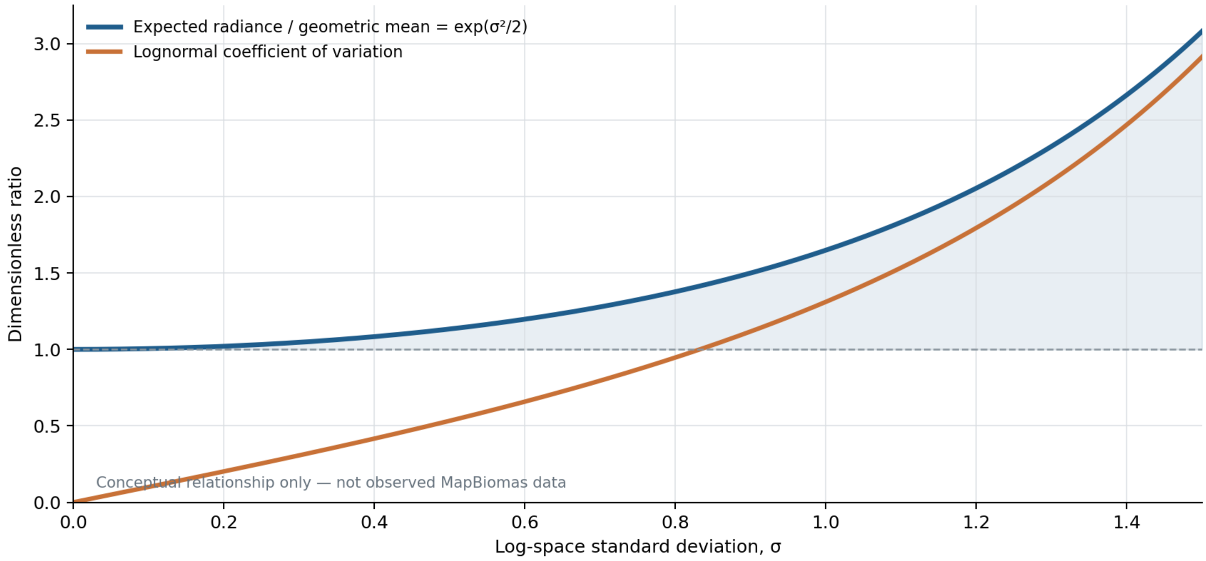

Figure 2. Conceptual effect of log-space dispersion on the lognormal expected-radiance correction and coefficient of variation. Curves are mathematical relationships, not observed product results.

For two annual products, the lognormal formulation also permits an exact decomposition of the change in expected radiance:

$$\Delta \ln(L) = \Delta\mu w + ½\Delta s_v{}^2$$

where $\Delta\mu w$ represents the change in central weighted log-radiance and $½\Delta s_v^2$ represents the contribution associated with the change in within-year multiplicative dispersion. This decomposition is descriptive rather than causal: it separates two statistical components of the annual radiance change but does not assign their physical origin.

The model-based relative dispersion is:

$$lognormal\_CV = \sqrt{[exp(s_v{}^2) - 1]}.$$

The implementation also provides a diagnostic standard error $SE(mu_w) = sqrt(s_w^2/n_{eff})$ and conditional 95% bounds:

$$CI95 = R_0\ exp[\mu w \pm 1.96\ SE(\mu w) + s_v{}^2 / 2].$$

The interval is conditional on the selected observations, reliability weights and estimated log variance. It does not include every component of retrieval, calibration, resampling or temporal-autocorrelation uncertainty.

Empirical inlier median, 10th percentile and 90th percentile are calculated alongside the model-based outputs. These bands provide direct distribution summaries without requiring the lognormal expectation to be used in every application.

3.6. Post-Processing, Grid Alignment and Export

The estimator outputs are assembled in a fixed 18-band order, converted to floating-point storage and clipped to the Brazil boundary. One image is exported for every complete calendar year. The output contains no temporal smoothing, change classification, spatial enhancement or fusion with a second sensor.

The source VNP46A2 grid is 15 arc seconds and is commonly described as nominal 500 m. Collection 1 uses a 250 m target grid for MapBiomas alignment. No bilinear or bicubic resampling call is made; Earth Engine therefore uses nearest-neighbour allocation unless the production configuration explicitly changes the kernel (Google Earth Engine, 2026b). This procedure assigns source values to the target grid and does not create additional spatial information.

The default public configuration uses EPSG:5880 and 250 m spacing. Operational production may supply the exact canonical MapBiomas affine transform through --crs-transform, which fixes pixel size, origin and alignment. Earth Engine asset and Cloud-Optimized GeoTIFF exports are supported using the documented export interfaces (Google Earth Engine, 2026c). GeoTIFF export uses -9999 as nodata after masking and clipping.

Each annual image receives metadata for year, temporal interval, source dataset and DOI, source radiance band, source support, output grid statement, resampling statement, radiance unit, quality schema, algorithm version and serialized parameter set.

3.6.1. Relationship wit MapBiomas LULC products

MapBiomas Brazil Nighttime Radiance Collection 1 is produced independently from the MapBiomas land-use and land-cover (LULC) classification products. LULC classes, thematic maps, demographic variables, infrastructure layers, or other environmental predictors are not used as inputs to the nighttime-radiance estimator, and the resulting radiance values do not modify or constrain the categorical LULC classifications. The annual nighttime-radiance product should therefore be interpreted as an independent continuous radiometric layer rather than as a component of the LULC classification workflow

The 250 m output grid is used to facilitate spatial compatibility with the MapBiomas analytical environment, while preserving the native information content of the VIIRS source data. This spatial alignment enables subsequent overlay and joint analysis with MapBiomas LULC products, for example to examine nighttime-radiance patterns across urban areas, agricultural landscapes, infrastructure corridors, or different land-cover classes. Such analyses are performed after production of the radiance maps and do not contribute to the estimation of annual radiance itself.

Accordingly, relationships between nighttime radiance and land-use or land-cover dynamics should be considered downstream analytical applications of Collection 1 rather than part of its map-generation algorithm. This separation preserves the independence of the radiometric product while allowing it to be integrated with MapBiomas LULC datasets as a complementary continuous layer for environmental, territorial, and urban analyses.

3.7. Software Implementation and Reproducibility

The public implementation described in §2.1.3 is versioned and parameterized for reproducible production. User-specific credentials and resource identifiers remain outside the scientific release specification. For each production release, the implementation records:

- software version and source-code revision;
- complete scientific parameter configuration;
- source dataset and annual source-image counts;
- output-band schema and order;
- boundary version and output-grid definition;
- numerical and configuration test results; and
- public and controlled production manifests.

The code applies one parameter object within each run. Reproducibility across independently processed years requires confirmation that all annual manifests contain the same canonical parameter-configuration hash. Appendix C defines the minimum release provenance.

4. Validation Strategies

4.1. Validation Framework

Validation is adapted to a continuous radiance product. There are no discrete reference labels, mapped classes, training samples or classification probabilities. Traditional overall, user's and producer's accuracies are therefore not applicable. Quality assessment instead examines whether the source observations, annual estimator, output grid and metadata behave as specified.

The Collection 1 framework combines four forms of evidence:

- verification of source-band and quality-flag semantics;
- internal statistical and temporal-support diagnostics;
- comparison with independent annual VIIRS composite products; and
- verification of software configuration, equations, output schema and exports.

This framework was executed for Collection 1 Version 1.0 and is reported in Supplementary Validation Report S1. The empirical panel comprises 192 fixed native-support locations distributed across six geographically separated Brazilian domains and four radiance strata. The same coordinates were evaluated in 2019, 2021 and 2024, producing 576 point-years and 206,624 archived VNP46A2 point-day observations.

4.2. Reference products

NASA VNP46A4 Collection 2 and Earth Observation Group (EOG) VIIRS nighttime-light products are methodologically relevant external comparison layers for overlapping years. They are not treated as error-free reference truth because their screening rules, temporal compositing, snow treatment, radiance thresholds and statistical estimands differ from those of Collection 1.

For Collection 1 Version 1.0, the executed external comparison reported in Supplementary Validation Report S1 used the EOG monthly VIIRS VCMSLCFG product annualised using cloud-free coverage. Across 576 matched point-years, the comparison yielded Spearman $\rho = 0.117$ and substantial brightness-dependent residual structure. This weak agreement is interpreted as evidence that the two VIIRS processing chains are not interchangeable; it is not interpreted as external accuracy confirmation. A separately executed VNP46A4 comparison is not part of the present validation evidence and should therefore not be implied.

No national field-reference product provides a direct, calibrated and spatially matched record of upward VIIRS-band radiance for all Brazilian locations and all years from 2013 to 2025. Ground illuminance, photographs and sky-brightness measurements observe different physical quantities and cannot be used as direct labels without spectral, angular, temporal and spatial-support matching.

4.3. Internal Quality Assessment

The following checks define the internal annual quality-assessment procedure:

1. confirm that the source collection, DOI, band names and packed-bit interpretation match VNP46A2 Collection 2;

2. confirm complete calendar-year filtering and record the number of source images;

3. inspect n_candidate, n_inlier, n_eff, candidate_fraction, valid_fraction and outlier_fraction before interpreting radiance;

4. verify that expected_radiance, percentiles and intervals are masked where effective support is insufficient;

5. compare expected radiance with weighted geometric mean, empirical median and percentiles on representative radiance profiles;

6. inspect high-dispersion and low-support locations separately from well-supported stable locations;

7. confirm identical parameters, band order, units, nodata handling and metadata for all years;

8. verify the target CRS, pixel size, origin, alignment, clipping and nearest-neighbour allocation; and

9. run the local configuration and numerical reference tests supplied with the repository.

Temporal comparability is supported by applying the same observation model and parameters to every year. This standardization reduces method-induced differences but does not remove changes in the number, season or geometry of valid observations. Annual comparison therefore requires the support bands defined in Appendix A. The internal procedures were additionally challenged through the empirical experiments reported in Supplementary Validation Report S1. These included direct annual-estimator agreement, distribution-quantile calibration, leave-one-month-out temporal representativeness, seven-day moving-block bootstrap uncertainty, QA-weight diagnostics, parameter sensitivity, component ablation and effective-support convergence. The results are summarized in §4.4.

4.4. Empirical Estimator Validation

Collection 1 was empirically validated using 192 fixed native-support locations distributed across six geographically separated Brazilian stress-test domains: Belo Horizonte, Brasília, Manaus, Porto Alegre, Recife and São Paulo. Sampling was stratified using four 2024 radiance regimes: 0.10–1, 1–5, 5–20 and ≥20 nW cm^{-2} sr^{-1}. Eight locations were retained in each stratum within each domain. The same fixed coordinates were evaluated in 2019, 2021 and 2024, producing 576 point-years from 206,624 archived VNP46A2 point-day observations. The panel was designed to challenge the estimator across different radiance, climatic, seasonal and urbanisation regimes; it is a stratified stress-test design rather than a probability sample of every Brazilian pixel or biome.

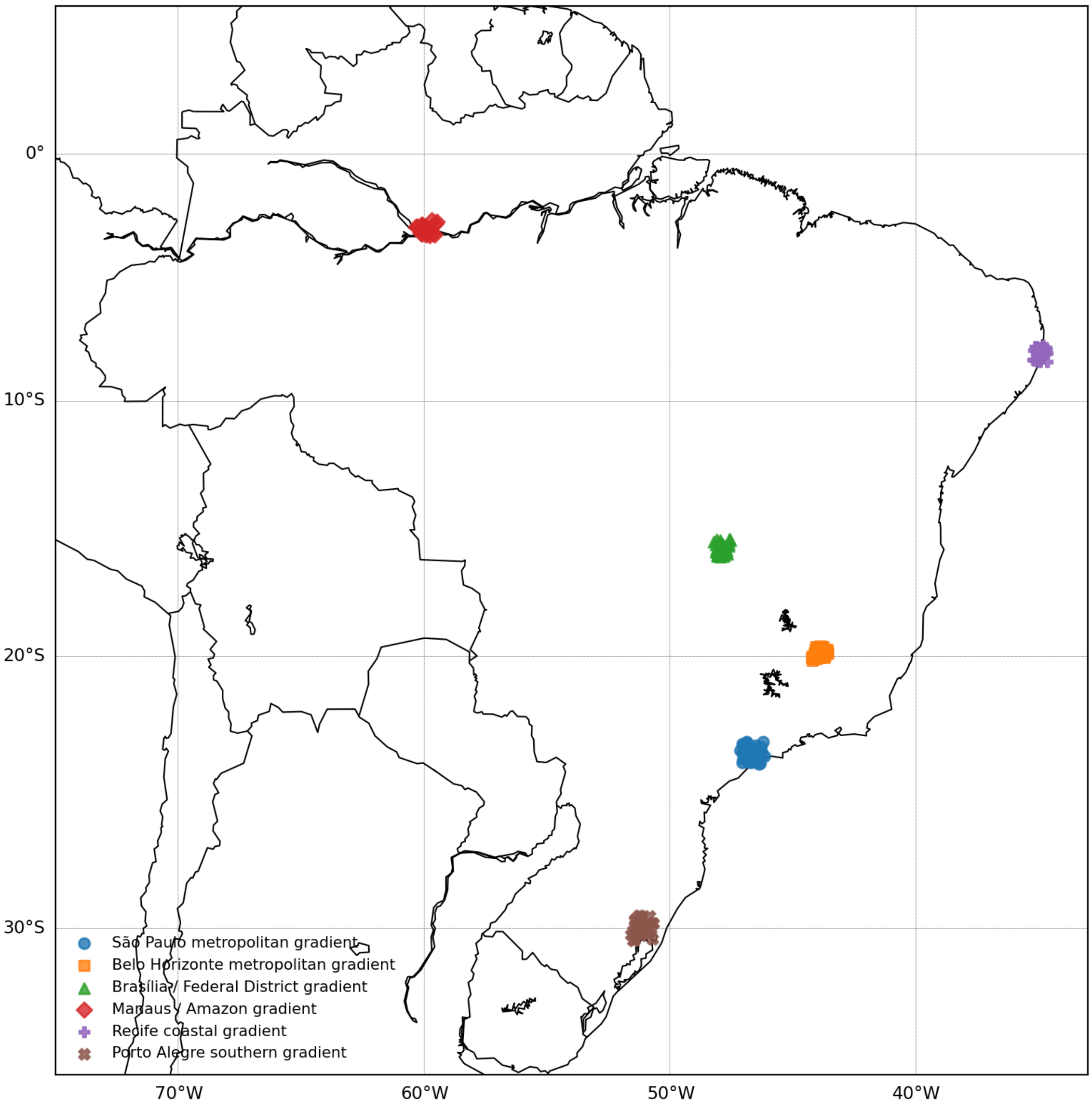

Figure 3. Spatial distribution of the 192 fixed validation locations across six Brazilian stress-test domains.

The primary validation examined whether the lognormal back-transformation materially changes the annual radiance magnitude relative to the empirical weighted arithmetic expectation calculated from the same retained daily observations and effective weights. Across all 576 point-years, the median absolute discrepancy was 0.40%, the 90th percentile was 1.83% and the 95th percentile was 2.74%. The median observed weighted coverage of the model-implied P10–P90 interval was 0.800 and the median absolute central-80% calibration error was 0.021. Median discrepancy remained below 0.66% in every validation domain and below 0.48% in every radiance stratum.

Temporal robustness was evaluated using leave-one-month-out omission. This experiment measures the representativeness of the annual estimate when part of the within-year record is absent; it is not interpreted as forecasting because a withheld month may differ legitimately owing to seasonal, temporary or structural changes in emitted light. The proposed lognormal formulation and weighted arithmetic expectation showed essentially identical median absolute log discrepancies (0.14277 and 0.14255, respectively). The result therefore provides no basis for ranking the estimators by predictive performance. Instead, it shows that retaining the lognormal distributional structure does not materially alter temporal representativeness relative to the direct weighted annual mean.

The additional value of the lognormal formulation lies in its information content. The estimator explicitly retains weighted log-location μw and within-year log variance s_v^2 and propagates the latter into expected radiance through $\exp(s_v^2/2)$. Removing this variance correction and reverting to the weighted geometric level changed annual radiance by 11.61% in median absolute terms. The formulation also permits the exact interannual decomposition $\Delta\ln(L) = \Delta\mu w + 0.5\Delta s_v^2$. In the 384 archived interannual transitions, the dispersion component accounted for at least 10% of the absolute two-component decomposition in 52.9% of transitions and at least 25% in 23.4%. Thus, similar changes in annual radiance may arise from different combinations of a shift in central radiance and a change in within-year variability.

Temporal dependence was evaluated with a seven-day moving-block bootstrap. Bootstrap 95% intervals were 1.124 times wider than the analytical conditional intervals on median, demonstrating that ci95_low and ci95_high should be interpreted as conditional model intervals rather than as a complete uncertainty envelope. Effective-support convergence further identified n_eff = 120 as the first tested high-stability tier for which the 90th-percentile subsampling error fell below 5%; at this threshold the P90 error was 4.45% and 92.6% of subsample estimates were within 5% of the full-year estimate. The production requirement n_eff ≥ 2 remains the mathematical computability threshold and should not be confused with this empirical high-stability interpretation tier.

The present validation establishes quantitative evidence for estimator behaviour, implementation, temporal support and conditional uncertainty under the tested conditions. It does not constitute absolute field-radiometric validation because no spectrally, angularly, temporally and spatially matched upward-radiance reference was available. It also does not constitute a probability-representative accuracy census of all Brazilian pixels. Full mathematical definitions, sampling coordinates, results, figures, sensitivity experiments and reproducibility records are provided in Supplementary Validation Report S1.

5. Map Collections and Analysis

5.1. Collection Summary

Collection	Period	Product	Core method	Quality assessment
Collection 1, version 1.0	2013-2025	Annual continuous nighttime radiance and support bands	VIIRS-only QA screening, log-space MAD filtering and quality-weighted lognormal estimation	Source-schema verification; 192-location, 576-point-year empirical estimator validation; distribution calibration; temporal-support and moving-block-bootstrap uncertainty assessment; parameter sensitivity and component ablation; EOG cross-product consistency; grid and software verification. Full results: Supplementary Validation Report S1.

Collection 1 is the first national release produced using the uniform method and fixed output schema documented in §§3.1-3.7.

5.2. Product Evolution and Versioning

Collection 1, Version 1.0 is the first dedicated release of the MapBiomas Brazil Nighttime Radiance product and therefore represents its baseline release. As no previous Nighttime Radiance collection exists, there is no earlier product version for direct methodological or temporal comparison. Collection 1 establishes the baseline dataset, output-band schema and public processing workflow against which subsequent releases will be documented.

A future update will receive a new version when it changes the source collection, platform, quality interpretation, thresholds, weights, estimator, time range, grid, resampling rule or band definition. Reprocessing earlier years with a changed method will be identified explicitly rather than replacing the historical series without documentation.Future versions may extend temporal coverage and evaluate continuity across VIIRS platforms. Any platform combination requires versioned inter-platform calibration and consistency assessment. The direct-radiance and VIIRS-only production boundary should be retained unless a separately named product documents a different measurement model.

5.3. Data and Code access

MapBiomas Brazil information, collections and download guidance are available at https://brasil.mapbiomas.org/en/ and https://brasil.mapbiomas.org/en/downloads/. The public Python workflow is prepared for distribution through https://github.com/mapbiomas-brazil. The repository contains the processing script, README, dependency files, example command, tests, licence and launch-announcement text.

6. Practical Considerations

6.1. Applications and Use

The annual series provides a standardized national layer for studying the distribution and evolution of satellite-observed nighttime radiance. It can support urban and infrastructure monitoring, regional planning, descriptive environmental analysis and integration with other MapBiomas products. Because the product is continuous, users may define application-specific summaries without modifying the original radiance layer.

Recommended analytical practice is to use expected_radiance together with at least one observation-support band. n_eff describes the effect of unequal weights, valid_fraction describes retained temporal coverage, and log_variance describes within-year dispersion after screening. The empirical median and percentiles provide useful alternatives when a non-parametric summary is preferred.

6.2. Operational Considerations

National processing of daily data is computationally intensive. Earth Engine performs the pixelwise reductions on the server, while the Python client defines the annual images and export tasks. Processing one calendar year per export improves task management and allows an incomplete or failed year to be rerun without rebuilding the complete series.

The public code requires user configuration because Earth Engine project and asset identifiers belong to the executing organization. The repository intentionally contains placeholders rather than deployable private resource names. Exact MapBiomas production runs should additionally use the canonical target-grid transform and retain internal provenance for the boundary asset and released asset IDs.

6.3. Methodological Advantages

The principal methodological properties established in §§3.3–3.7 can be summarized as follows:

- one documented observation model for the full 2013-2025 series;
- direct use of NASA-corrected radiance without auxiliary thematic predictors;
- robust reduction of gross residual departures in multiplicative log space;
- graded use of accepted observation quality rather than a single unweighted mean;

- explicit distinction between log variance and log standard deviation;
- effective sample size and coverage layers distributed with radiance;
- empirical percentiles alongside the model-based expectation;
- empirical confirmation that the lognormal annual expectation preserves annual radiance magnitude relative to the direct weighted arithmetic expectation, with a median absolute discrepancy of 0.40% and P90 of 1.83%, while retaining explicit within-year multiplicative dispersion;
- exact separation of annual expected radiance into weighted log-location and log-dispersion components, including the interannual identity, which allows changes in central radiance and changes in within-year variability to be distinguished statistically.
- reproducible annual exports with machine-readable metadata.

6.4. Limitations and Uncertainty

Several characteristics define the appropriate interpretation of the collection.

First, VIIRS DNB has a broad panchromatic spectral response and observes upward radiance near the satellite overpass time. Lighting technologies with different spectra may not produce proportional DNB responses, and the product does not directly measure ground-level illuminance or ecological exposure (Levin et al., 2020).

Second, accepted radiance variability contains both real changes in emitted light and residual observation effects. Atmospheric correction, viewing geometry, surface reflectance, geolocation and retrieval uncertainty can contribute to within-year dispersion (Wang et al., 2021; Tan et al., 2021). log_variance therefore describes the dispersion of accepted VIIRS observations, not a uniquely identified cause.

Third, the lognormal expectation is a statistical model for positive radiance. Intermittent or mixed sources may produce distributions that are not well represented by one lognormal profile. The collection retains the median and empirical percentiles so that users can inspect or select less model-dependent summaries.

Fourth, the reliability weights are explicit Collection 1 QA parameters. The validation showed that the ordering of the assigned QA weights was consistent with the observed residual-variance ordering (Spearman $\rho = 0.866$). However, almost all eligible observations in the validation panel received the maximum weight ($q = 1.0$), so the available data do not provide a strong empirical basis for calibrating the exact numerical differences between QA weights. Kish effective sample size, n_eff, accounts for unequal weights but not for temporal dependence between consecutive observations.

Fifth, the 0.10 nW cm^-2 sr^-1 floor permits logarithmic processing and does not establish that every retained low value represents detected artificial lighting. Interpretation near the radiometric background requires particular attention to coverage and dispersion.

Finally, the 250 m output grid is finer than the nominal 500 m source grid. Nearest-neighbour allocation supports grid compatibility but does not add spatial detail. Adjacent 250 m cells may inherit the same source observation and should not be treated as independent high-resolution measurements.

6.5. Perspectives

Future work can strengthen the collection through systematic cross-platform consistency analysis, independent radiometric reference sites, sensitivity analysis of the reliability weights and lunar threshold, and block-based uncertainty estimates that account for temporal dependence. These improvements can be introduced within the same documented product framework and recorded as new versions.

7. Concluding Remarks and Perspectives

MapBiomas Brazil Nighttime Radiance Collection 1 provides a consistent annual record of VIIRS DNB upward nocturnal radiance for Brazil from 2013 to 2025. It transforms daily NASA Black Marble VNP46A2 observations into annual maps through explicit quality screening, robust log-space filtering and a quality-weighted lognormal estimator. Radiance and its observation-support context are delivered together in the fixed schema defined in Appendix A.

Empirical validation supports the annual estimator as a distribution-aware representation of nighttime radiance. The lognormal expectation preserves annual radiance magnitude closely relative to the empirical weighted arithmetic expectation while additionally retaining explicit information on within-year multiplicative dispersion and effective temporal support. This distinction allows locations or years with similar annual radiance magnitude but different temporal radiance structures to remain distinguishable in the distributed product.

The product is designed for transparent integration with MapBiomas. It is based only on VIIRS radiance and internal VIIRS quality information, uses one national configuration for every year and records the information needed to reproduce the annual exports. The 250 m distributed grid supports alignment with MapBiomas while preserving the nominal 500 m information support of the source product.

Collection 1 establishes the methodological and software baseline for future releases. Extensions of the time series, changes in VIIRS platform or revisions to parameters and grids will be documented through versioned updates to the data, code and ATBD.

8. References

Aitchison, J. and Brown, J.A.C. (1957). The Lognormal Distribution. Cambridge University Press.

Elvidge, C.D., Baugh, K., Zhizhin, M., Hsu, F.-C. and Ghosh, T. (2017). VIIRS night-time lights. International Journal of Remote Sensing, 38(21), 5860-5879. https://doi.org/10.1080/01431161.2017.1342050.

Elvidge, C.D., Zhizhin, M., Ghosh, T., Hsu, F.-C. and Taneja, J. (2021). Annual time series of global VIIRS nighttime lights derived from monthly averages: 2012 to 2019. Remote Sensing, 13(5), 922. https://doi.org/10.3390/rs13050922.

Google Earth Engine (2026a). VNP46A2: VIIRS Lunar Gap-Filled BRDF Nighttime Lights Daily L3 Global 500 m. Dataset catalogue. https://developers.google.com/earth-engine/datasets/catalog/NASA_VIIRS_002_VNP46A2.

Google Earth Engine (2026b). Resampling and reducing resolution. https://developers.google.com/earth-engine/guides/resample.

Google Earth Engine (2026c). Exporting images. https://developers.google.com/earth-engine/guides/exporting_images.

Kish, L. (1965). Survey Sampling. John Wiley & Sons.

Levin, N., Kyba, C.C.M., Zhang, Q., Sánchez de Miguel, A., Román, M.O., Li, X., Portnov, B.A., Molthan, A.L., Jechow, A., Miller, S.D., Wang, Z., Shrestha, R.M. and Elvidge, C.D. (2020). Remote sensing of night lights: a review and an outlook for the future. Remote Sensing of Environment, 237, 111443. https://doi.org/10.1016/j.rse.2019.111443.

NASA VIIRS Land Science Investigator-led Processing System (2024a). Black Marble User Guide, Collection 2.0. NASA. https://landweb.modaps.eosdis.nasa.gov/data/userguide/BlackMarbleUserGuide_Collection2.0_20241203.pdf.

NASA VIIRS Land Science Investigator-led Processing System (2024b). VIIRS/NPP Gap-Filled Lunar BRDF-Adjusted Nighttime Lights Daily L3 Global 15 arc-second Linear Lat Lon Grid, Collection 2. https://doi.org/10.5067/VIIRS/VNP46A2.002.

Román, M.O., Wang, Z., Sun, Q., Kalb, V., Miller, S.D., Molthan, A., Schultz, L., Bell, J., Stokes, E.C., Pandey, B., Seto, K.C., Hall, D., Oda, T., Wolfe, R.E., Lin, G., Golpayegani, N., Devadiga, S., Davidson, C., Sarkar, S., Praderas, C., Schmaltz, J., Boller, R., Stevens, J., Ramos González, O.M., Padilla, E., Alonso, J., Detrés, Y., Armstrong, R., Miranda, I., Conte, Y., Marrero, N., MacManus, K., Esch, T. and Masuoka, E.J. (2018).

NASA's Black Marble nighttime lights product suite. Remote Sensing of Environment, 210, 113-143. https://doi.org/10.1016/j.rse.2018.03.017.

Rousseeuw, P.J. and Croux, C. (1993). Alternatives to the median absolute deviation. Journal of the American Statistical Association, 88(424), 1273-1283. https://doi.org/10.1080/01621459.1993.10476408.

Small, C. (2021). Spatiotemporal characterization of VIIRS night light. Frontiers in Remote Sensing, 2, 775399. https://doi.org/10.3389/frsen.2021.775399.

Tan, X., Zhu, X., Chen, J. and Chen, R. (2021). Modeling the direction and magnitude of angular effects in nighttime light remote sensing. Remote Sensing of Environment, 269, 112834. https://doi.org/10.1016/j.rse.2021.112834.

Wang, Z., Román, M.O., Kalb, V.L., Miller, S.D., Zhang, J. and Shrestha, R.M. (2021). Quantifying uncertainties in nighttime light retrievals from Suomi-NPP and NOAA-20 VIIRS Day/Night Band data. Remote Sensing of Environment, 263, 112557. https://doi.org/10.1016/j.rse.2021.112557.

Wang, Z., Shrestha, R.M., Román, M.O. and Kalb, V.L. (2022). NASA's Black Marble multiangle nighttime lights temporal composites. IEEE Geoscience and Remote Sensing Letters, 19, 2505105. https://doi.org/10.1109/LGRS.2022.3176616.

Zheng, Q., Weng, Q., Zhou, Y. and Dong, B. (2022). Impact of temporal compositing on nighttime light data and its applications. Remote Sensing of Environment, 274, 113016. https://doi.org/10.1016/j.rse.2022.113016.

APPENDIX A. MapBiomas Network

General Coordinator
Camila Palhares Teixeira

Technical Coordinator
Pawel Tysiac
Vinicius Donisete Lima Rodrigues Goulart

Scientific/Technical Coordination:
Pawel Tysiac
Vinicius Donisete Lima Rodrigues Goulart
Camila Palhares Teixeira

Team
Julio Cesar Pedrassoli
Marcos Rosa
Júlia Shimbo
Edimilson Rodrigues

Institutional affiliations: State University of Minas Gerais (UEMG) / Gdansk University of Technology/MapBiomas Brazil/EESC-USP

The research is supported by FAPEMIG APQ-05944-24 and the European Union under the Horizon Europe Programme, Grant Agreement No. 101135308 (PLAN-B).

Contact
Pawel Tysiac - pawel.tysiac@pg.edu.pl
Camila Teixeira camila.teixeira@uemg.br

How to cite
MapBiomas Brazil Nighttime Radiance Team. 2026. MapBiomas Brazil Nighttime Radiance Collection 1: Algorithm Theoretical Basis Document, Version 1.0. MapBiomas Brazil.

APPENDIX B Output band dictionary

Band	Unit	Description	Use
`expected_radiance`	nW cm^-2 sr^-1	Quality-weighted lognormal annual expectation	Principal annual radiance layer
`weighted_mean_log_radiance`	Dimensionless	Weighted mean of `ln(R/R0)`	Log-space location
`log_variance`	Dimensionless squared	Effective-sample-corrected weighted log variance	Within-year log dispersion
`log_standard_deviation`	Dimensionless	Square root of log variance	Log-space standard deviation
`lognormal_cv`	Dimensionless	`sqrt(exp(log_variance) - 1)`	Model-based relative dispersion
`median_radiance`	nW cm^-2 sr^-1	Median of retained daily radiances	Robust empirical location
`p10_radiance`	nW cm^-2 sr^-1	10th percentile of retained daily radiances	Lower empirical distribution summary
`p90_radiance`	nW cm^-2 sr^-1	90th percentile of retained daily radiances	Upper empirical distribution summary
`n_eff`	Effective observations	Kish effective sample size after weighting	Weighted observation support
`n_candidate`	Observations	Count after VIIRS QA and before MAD screening	Candidate support
`n_inlier`	Observations	Count after MAD screening	Retained support
`candidate_fraction`	Proportion	Candidate observations divided by calendar days	Pre-MAD temporal coverage
`valid_fraction`	Proportion	Inlier observations divided by calendar days	Retained temporal coverage
`outlier_fraction`	Proportion	MAD-rejected candidates divided by candidate count	Robust-screening diagnostic
`mean_reliability`	Dimensionless	Mean candidate reliability score	Average accepted-observation quality
`mean_retrieval_age_days`	Days	Mean VNP46A2 retrieval-age value for candidates	Source provenance diagnostic
`ci95_low`	nW cm^-2 sr^-1	Lower conditional 95% bound	Diagnostic model interval
`ci95_high`	nW cm^-2 sr^-1	Upper conditional 95% bound	Diagnostic model interval

APPENDIX C. Collection 1 parameter configuration

Parameter	Default	Role
Start year	2013	First annual map
End year	2025	Last annual map in Collection 1
Minimum radiance	0.10 nW cm^-2 sr^-1	Positive floor before logarithm
Maximum lunar irradiance	30	Conservative lunar screening
Minimum cloud-mask quality	1	Accepts low, medium and high mask quality
Maximum cloud confidence	1	Accepts confident clear and probably clear
Probably-clear weight	0.70	Cloud-confidence reliability component
Low cloud-mask-quality weight	0.80	Mask-quality reliability component
Uncertainty floor	0.03	Minimum nominal log-space uncertainty
Uncertainty range	0.30	Reliability-dependent uncertainty component
MAD multiplier	3.5	Robust log-space inlier threshold
Minimum effective observations	2.0	Minimum support for expected radiance and interval
Surface filter	None	National boundary defines export domain
Output CRS	EPSG:5880 by default	Replaceable by canonical MapBiomas CRS
Output grid spacing	250 m	Grid alignment, not spatial enhancement
Resampling	Nearest neighbour	Preserves source cell values during allocation

APPENDIX D. Reproducibility Metadata

Each production release records the following information in the image properties, public run manifest or controlled production log:

- software version and source-code revision;
- VNP46A2 dataset identifier, collection and DOI;
- inclusive processing years and exact annual date ranges;
- direct science band and internal VIIRS quality bands;
- all observation-screening, weighting and estimator parameters;
- source-image count for each annual period;
- output-band order, units, data type and nodata value;
- output CRS, affine transform or scale, pixel origin and resampling rule;
- national boundary version used for clipping;
- annual export status and destination recorded in the controlled production environment; and
- results of configuration, numerical-reference, schema, spatial-alignment and visual product checks.
- The public manifest omits credentials, authentication tokens, Cloud project identifiers, Earth Engine asset identifiers, Earth Engine task identifiers and local paths.

Validation reproducibility

Validation Supplement: Supplementary Validation Report S1, Version 1.0
Validation years: 2019, 2021, 2024
Sampling year: 2024
Validation domains: Belo Horizonte, Brasília, Manaus, Porto Alegre, Recife, São Paulo
Unique fixed locations: 192
Radiance strata per domain: 4
Locations per stratum per domain: 8
Archived VNP46A2 point-day rows: 206,624
Moving-block length: 7 days
External comparison dataset: NOAA/VIIRS/DNB/MONTHLY_V1/VCMSLCFG

SUPPLEMENTARY VALIDATION REPORT S1 - Empirical validation of the MapBiomas Brazil Nighttime Radiance Collection 1 annual VIIRS DNB estimator

S1. Validation objective and scope

The objective of this supplementary analysis is to quantify the behaviour of the Collection 1 annual compositing estimator under geographically, radiometrically and temporally contrasting conditions. The validation evaluates annual radiance magnitude, distributional calibration, temporal representativeness, uncertainty under temporal dependence, parameter sensitivity, component contributions and effective observation support.

The validation target is the annual compositing estimator and the information carried by its accompanying support and dispersion variables. All experiments use the same VNP46A2 direct-radiance observations and Collection 1 screening rules as the released product.

S2. Validation data, domains and sample design

S2.1 Source observations

The validation uses the same NASA Black Marble VNP46A2 Collection 2 daily product as the released estimator (Google Earth Engine collection NASA/VIIRS/002/VNP46A2; DOI 10.5067/VIIRS/VNP46A2.002). The direct DNB_BRDF_Corrected_NTL band is the radiometric source. Internal VNP46A2 quality variables are used for screening and reliability weighting. The gap-filled radiance band is not part of the primary estimator.

The validation dataset contains 206,624 sampled point-day observations across six Brazilian validation domains in 2019, 2021 and 2024. After application of the Collection 1 candidate rules, 58,364 observations satisfy the eligibility criteria before MAD screening. Annual estimation is performed independently for each point-year, giving 576 point-years.

S2.2 Validation domains

Domain	Bounding box	Stress-test rationale
Belo Horizonte metropolitan gradient	-44.25 to -43.55° lon; -20.20 to -19.55° lat	southeastern urban-rural gradient used in the pilot
Brasília / Federal District gradient	-48.25 to -47.45° lon; -16.15 to -15.45° lat	Cerrado, planned urban form and broad low-to-moderate radiance
Manaus / Amazon gradient	-60.55 to -59.45° lon; -3.45 to -2.65° lat	humid tropical / cloud-prone Amazon setting with sharp city-forest contrast
Porto Alegre southern gradient	-51.65 to -50.65° lon; -30.45 to -29.55° lat	southern latitude, different seasonality and atmospheric regime
Recife coastal gradient	-35.25 to -34.65° lon; -8.45 to -7.75° lat	tropical coastal atmosphere, dense urban lighting and coastal geometry
São Paulo metropolitan gradient	-47.15 to -46.15° lon; -24.05 to -23.20° lat	very bright dense urban core plus peri-urban/rural fringe

The domains were selected to span distinct lighting, urban form, atmospheric and seasonal contexts: very bright dense metropolitan lighting, peri-urban/rural gradients, Cerrado conditions, humid tropical/cloud-prone Amazon conditions, tropical coastal geometry and southern-latitude seasonality. This is a coverage-oriented stress test rather than a claim of biome-proportional representativeness.

S2.3 Stratification and selection of validation locations

Sampling was anchored to the 2024 sampling year. Four radiance regimes were used to span the processing floor, low-radiance, moderate-radiance and bright conditions. Eight fixed native-support locations were retained in each stratum within each of six geographically separated domains, yielding 192 unique locations; the same coordinates were then reused in 2019, 2021 and 2024 (576 point-years). Figure S1 shows the actual spatial panel. The design is intentionally stratified and stress-test oriented rather than a probability sample of Brazil.

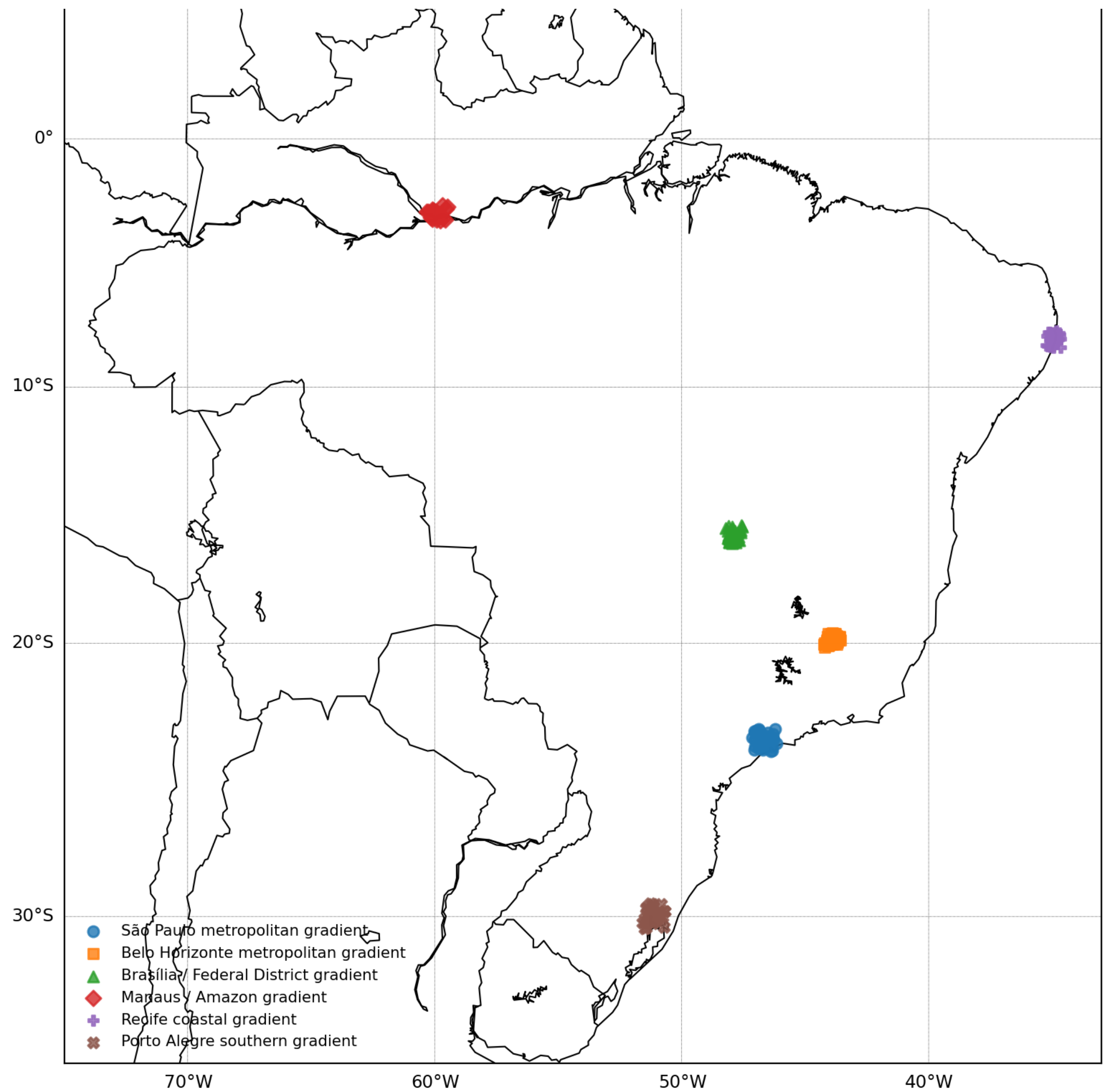

Figure S1. Spatial distribution of the 192 validation locations across six Brazilian domains and four radiance strata. The same coordinates were evaluated in 2019, 2021 and 2024.

Stratum	Definition/label	Locations	Min 2024 reference	Median	Max
1	dim 0.10 1	48	0.344	0.609	0.988
2	low 1 5	48	1.006	1.469	4.272
3	moderate 5 20	48	5.324	9.974	18.228
4	bright ge 20	48	20.046	47.118	88.000

S2.4 Observation support in the validation panel

Support quantity	Median	P10	P90	Minimum	Maximum
Candidate observations	105.5	57.0	139.0	30.0	158.0
MAD-retained observations	105.0	56.5	138.5	30.0	158.0
Kish n_eff	105.0	56.5	138.5	30.0	158.0
Candidate fraction	28.9%	15.6%	38.0%	8.2%	43.2%
MAD outlier fraction	0.0%	0.0%	1.6%	0.0%	11.4%

S3. Production estimator reproduced in validation

The validation reproduces the released Collection 1 estimator before testing its behaviour. The equations and fixed parameter values below follow the mathematical specification of the main ATBD.

S3.1 Candidate screening

Screening element	Collection-1 validation rule
Day/night flag	Night: QF_Cloud_Mask bit 0 = 0
Cloud-mask quality	Bits 4–5 ≥ 1
Cloud confidence	Bits 6–7 ∈ {0,1}: confident clear or probably clear
Cloud shadow	Bit 8 = 0
Cirrus	Bit 9 = 0
Snow/ice surface	Bit 10 = 0
Aurora	Bit 12 = 0
Lunar eclipse	Bit 13 = 0
Snow_Flag	0
Mandatory_Quality_Flag	0
DNB_Lunar_Irradiance	< 30
Direct radiance	> 0.10 nW cm^{-2} sr^{-1}

S3.2 Log transformation and robust inlier rule

$$x_i = \ln(R_i / R_0), \quad R_0 = 1\ nW\ cm^{-2}\ sr^{-1} \quad (1)$$

For each point-year, the candidate log-radiances are centred on their median m. MAD is the median absolute deviation. A robust scale is formed as max(1.4826·MAD, ε), where ε denotes the implementation safeguard against a zero scale. The Collection-1 inlier indicator is:

$$I_i = 1\{ |x_i - m| \le 3.5 \cdot \max(1.4826 \cdot MAD, \varepsilon) \} \quad (2)$$

S3.3 Reliability weights and effective sample size

Candidate reliability q_i is the product of cloud-confidence and cloud-mask-quality factors. Confident clear receives 1.00 and probably clear 0.70; medium/high cloud-mask quality receives 1.00 and low quality 0.80. The nominal log-space uncertainty penalty and effective weight are:

$$u_i = 0.03 + 0.30(1 - q_i) \quad (3)$$

$$w_i = I_i\, q_i / (1 + u_i^2) \quad (4)$$

$$\mu w = \Sigma_i\, w_i x_i / \Sigma_i\, w_i \quad (5)$$

$$n\_eff = (\Sigma_i\, w_i)^2 / \Sigma_i\, w_i^2 \quad (6)$$

S3.4 Weighted log variance and expected radiance

$$v\_b = \Sigma_i\, w_i(x_i - \mu w)^2 / \Sigma_i\, w_i \quad (7)$$

$$s\_v^2 = v\_b \cdot n\_eff/(n\_eff - 1), \quad n\_eff > 1 \quad (8)$$

$$L\_LN = R_0 \exp(\mu w + s\_v^2/2) \quad (9)$$

The released expected_radiance is therefore a quality-weighted lognormal expectation, not a geometric mean. The analytical interval in the ATBD is conditional on the retained observations, weights and estimated log variance; it is not a complete sensor/retrieval/serial-correlation uncertainty budget.

S4. Validation experiments and statistical definitions

S4.1 Direct validation of the lognormal annual expectation

For each point-year, the proposed lognormal expectation is compared with the empirical weighted arithmetic expectation computed from exactly the same retained daily observations and effective weights:

$$L\_emp = \Sigma_i\, w_i R_i / \Sigma_i\, w_i \quad (10)$$

$$D\_LN = 100 \cdot (L\_LN/L\_emp - 1)\ [\%] \quad (11)$$

This is a direct test of the practical consequence of the lognormal back-transformation. It does not claim that every log-radiance distribution is exactly Gaussian.

S4.2 Distribution-shape calibration

Mean agreement can conceal distributional misspecification. Therefore model-implied lognormal quantiles are compared with empirical weighted quantiles. For probability p and standard-normal quantile z_p:

$$Q_p^{LN} = R_0 \exp(\mu w + z_p s_v) \quad (12)$$

The validation compares P10, P50 and P90, and evaluates the weighted fraction of retained observations that falls within the model-implied P10–P90 interval:

$$C_{80} = \Sigma_i w_i \cdot 1\{Q_{0.1}^{LN} \le R_i \le Q_{0.9}^{LN}\}/\Sigma_i w_i \quad (13)$$

$$E_{80} = |C_{80} - 0.80| \quad (14)$$

A conventional normality test is retained as a diagnostic only; the assessment is based primarily on the model quantities that affect the released product. In the validation panel, 23.96% of point-years reject normality at $p<0.05$, so agreement of means and quantiles is evaluated directly rather than treating a normality p-value as a binary acceptance criterion.

S4.3 Leave-one-month-out temporal representativeness assessment

Each point-year is partitioned by calendar month. One month is omitted, the annual estimator is recomputed from the remaining months, and the resulting annual estimate is compared with the weighted radiance of the omitted month. This experiment measures within-year temporal representativeness and sensitivity to seasonal omission. It is deliberately not interpreted as forecasting: a real lighting change, temporary event or seasonal emission pattern may make the omitted month legitimately different from the remainder of the year.

$$e = \ln(L_{pred} / L_{holdout}) \quad (15)$$

$$|e| = \text{absolute log error} \quad (16)$$

The proposed estimator is compared with weighted arithmetic, weighted geometric, empirical median, unweighted lognormal and no-MAD lognormal alternatives. Monthly folds are first collapsed to point-year cluster medians so that the 12 omitted months are not treated as independent replicates. Cluster-bootstrap confidence intervals and Wilcoxon tests are then computed across the 576 point-year clusters. The 2% multiplicative margin is retained only as a practical equivalence/stability criterion, not as a claim of hold-out accuracy:

$$\delta_{NI} = \ln(1.02) = 0.0198026 \quad (17)$$

S4.4 Temporal-dependence-aware uncertainty

The production interval uses Kish effective sample size but does not model serial dependence. The validation therefore applies a moving-block bootstrap with 7-day blocks and 500 valid bootstrap replicates per point-year, preserving short temporal runs. Interval widths are compared by:

$$B = W_{bootstrap,95} / W_{parametric,95} \quad (18)$$

$B>1$ indicates that serial dependence and temporal structure produce wider uncertainty than the conditional analytical interval.

S4.5 QA-weight empirical ordering

The validation estimates robust log-residual variance by observed QA state and converts it to a relative inverse-variance reliability scale, normalised to a maximum of one. Spearman rank agreement between the fixed Collection-1 q values and empirical relative weights is used as an ordering diagnostic. It is not interpreted as sensor-level covariance calibration.

In the validation panel, 99.976% of eligible observations received q=1.0 and only 14 observations received q=0.7. The experiment therefore provides evidence on the ordering of QA weights, but only limited information for estimating the exact magnitude of the reduced weight.

S4.6 Parameter sensitivity and component ablation

One-at-a-time sensitivity perturbs the radiance floor, lunar-irradiance threshold, QA weights, uncertainty range and MAD multiplier while all other settings remain fixed. The change in annual expected radiance is expressed as:

$\Delta\_sens = 100 \cdot (L\_scenario/L\_base - 1)$ (19)

Ablation separately removes or replaces major algorithmic components: lognormal variance correction, QA weighting, MAD screening and the full estimator versus weighted arithmetic and robust median summaries.

S4.7 Effective temporal support and n_eff convergence

The production threshold n_eff≥2 is a mathematical threshold required to define the corrected variance; it is not an empirical stability criterion. The validation repeatedly forms month-block subsamples, re-estimates annual radiance and measures absolute relative error against the full-year estimator. The recommended high-stability threshold is the lowest tested n_eff at which the 90th percentile absolute subsampling error is ≤5%.

S4.8 External EOG consistency

An external processing-chain comparison is performed with the Earth Observation Group monthly VIIRS VCMSLCFG product, annualised using cloud-free coverage as weights. The EOG product uses a different compositing and screening workflow. Spearman correlation, median difference, median absolute difference, RMSE and log-ratio diagnostics are calculated to quantify agreement between the two processing chains.

S5. Results

S5.1 Overall numerical evidence

Quantity	Result	Interpretation
Unique fixed validation locations	192	6 domains × 4 radiance strata × 8 locations
Point-years	576	2019, 2021, 2024
Sampled point-day observations	206,624	raw VNP46A2 extraction returned by the run
Median |D_LN|	0.398%	lognormal vs empirical annual expectation
P90 |D_LN|	1.831%	90% of point-years below this discrepancy
Median central-80 calibration error	0.021	|observed weighted coverage − 0.80|
Median bootstrap/parametric CI width ratio	1.124×	moving-block bootstrap is wider on median
QA-weight Spearman ordering	0.866	ordering diagnostic; q<1 observations are rare
Recommended high-stability n_eff	120	P90 subsampling error ≤5%
External EOG Spearman rho	0.117	weak cross-product consistency; not truth

S5.2 Lognormal expectation and distribution calibration

Across all 576 point-years, median |D_LN| was 0.40% and P90 was 1.83%; P95 was 2.74%. The median observed weighted central-80 coverage was 0.800 and the median absolute calibration error was 0.021. These results support the practical use of $\exp(\mu w+s\_v^2/2)$ for the annual mean while showing that exact log-normality is not required at every point-year.

Figure S2. Proposed quality-weighted lognormal annual expectation versus the empirical weighted arithmetic expectation computed from the same retained daily VNP46A2 observations. The 1:1 line indicates numerical agreement of the annual mean estimand.

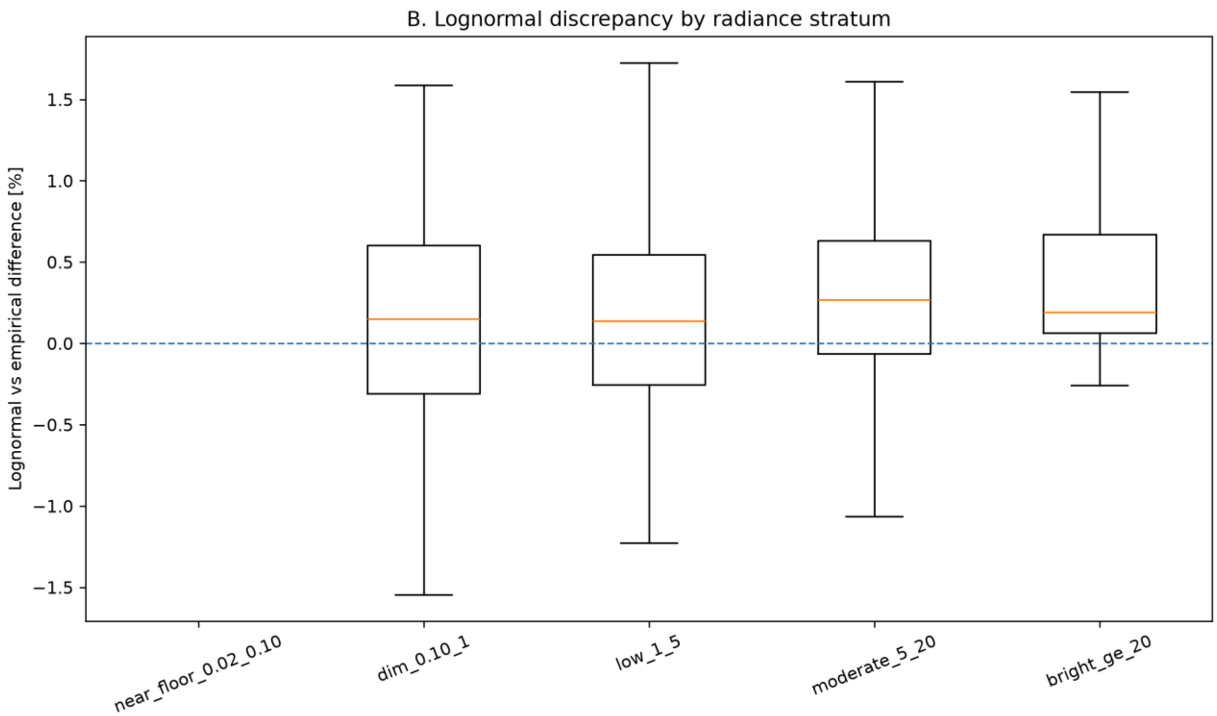

Figure S3. Percentage discrepancy D_LN between the lognormal expectation and empirical weighted expectation by radiance stratum. Systematic stratum dependence would indicate that the lognormal correction behaves differently across brightness regimes.

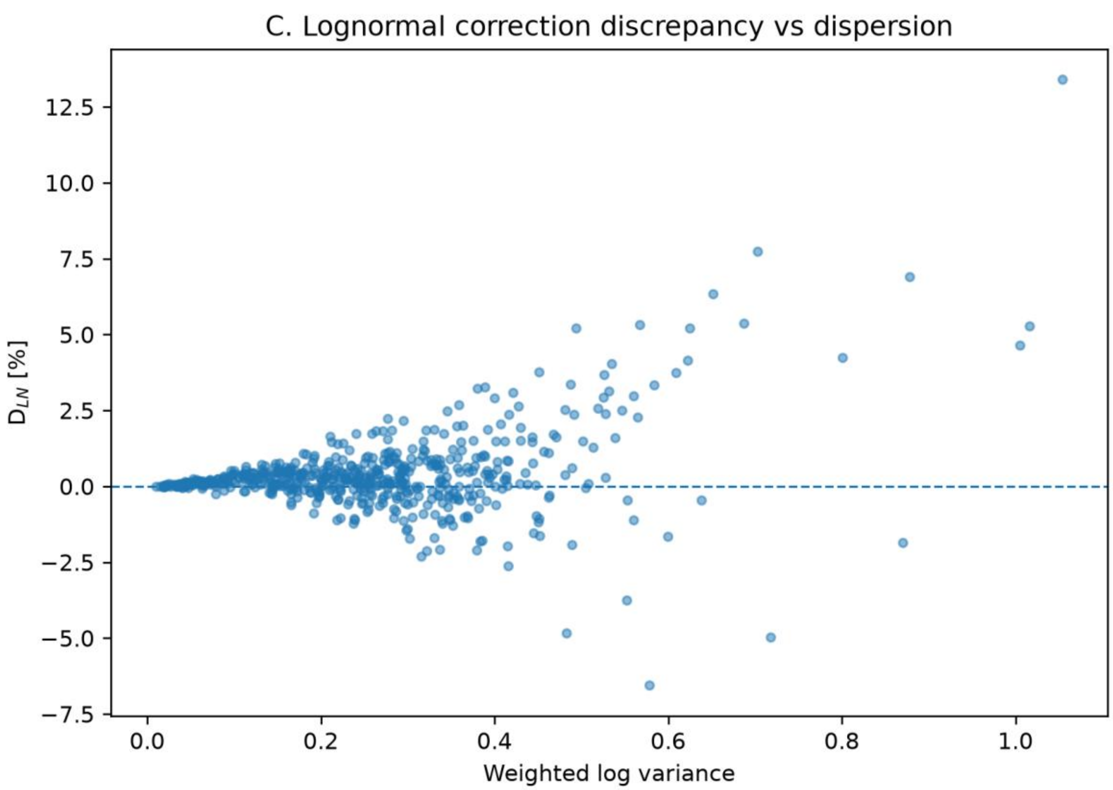

Figure S4. D_LN as a function of weighted log-space variance. Increasing multiplicative dispersion increases the potential difference between parametric and empirical annual expectations, but the central discrepancy remains small for most point-years.

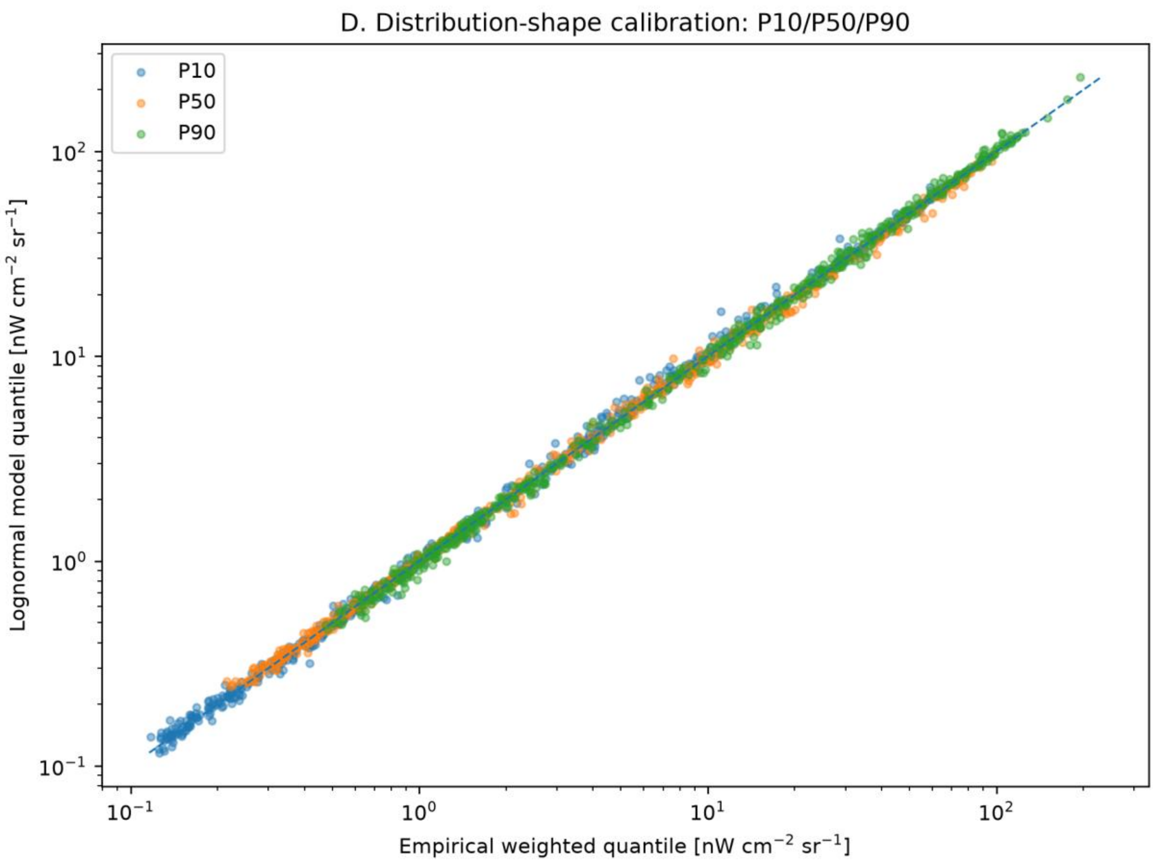

Figure S5. Model-implied P10, P50 and P90 against empirical weighted quantiles. This tests whether the assumed lognormal shape reproduces the retained daily distribution beyond the mean.

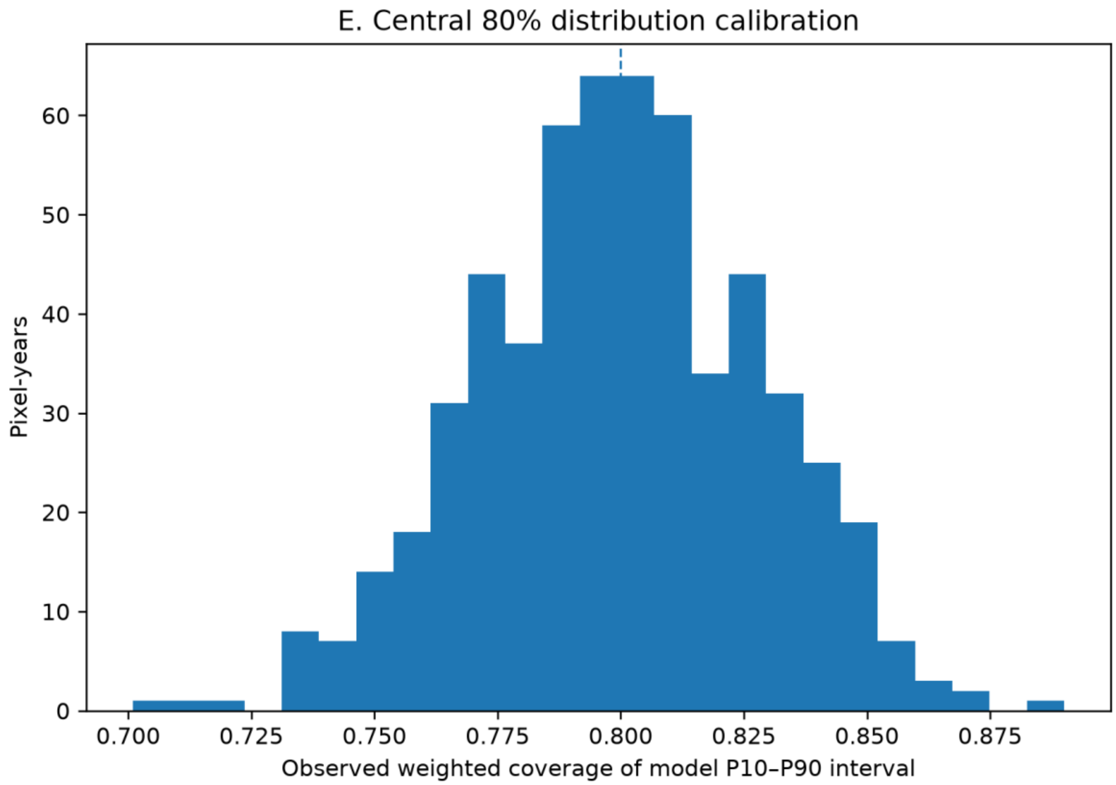

Figure S6. Weighted fraction of retained daily observations falling inside the model-implied P10–P90 interval. The distribution centres close to the nominal 0.80 coverage.

Radiance stratum	n	Median expected radiance	Median n_eff	Median |D_LN|	P90 |D_LN|
dim 0.10 1	144	0.522	98.0	0.476%	1.226%
low 1 5	144	1.454	108.0	0.407%	1.718%
moderate 5 20	144	9.833	105.0	0.436%	2.338%
bright ge 20	144	45.043	106.5	0.203%	1.963%

S5.3 Temporally blocked hold-out comparison

The leave-one-month-out temporal hold-out discrepancies are nearly identical for the proposed lognormal estimator and weighted arithmetic (median absolute log discrepancy 0.14277 and 0.14255, respectively). This tiny difference has no scientific meaning as a “winner”. The experiment instead shows that adding the lognormal distributional structure does not materially degrade temporal representativeness relative to the direct weighted annual mean.

Estimator	Folds	Median log bias	Median |log error|	RMSE log	Median |rel. error|	Within 20%
weighted_arithmetic	6555	0.01935	0.14255	0.25953	14.19%	63.1%
unweighted_lognormal	6555	0.02222	0.14277	0.26027	14.20%	63.0%
proposed_lognormal	6555	0.02222	0.14277	0.26027	14.20%	63.0%
no_mad_lognormal	6555	0.02308	0.14334	0.26201	14.30%	62.9%

Estimator	Folds	Median log bias	Median |log error|	RMSE log	Median |rel. error|	Within 20%
median	6555	-0.06998	0.15882	0.28570	15.47%	60.3%
weighted_geometric	6555	-0.07714	0.16172	0.27997	15.72%	61.0%

Competitor	Clusters	Median paired Δ	95% cluster-bootstrap CI	Proposed win rate	Non-inferior within 2%
weighted_geometric	576	-0.04124	[-0.05017, -0.02763]	71.0%	YES
median	576	-0.02170	[-0.03413, -0.01612]	68.4%	YES
unweighted_lognormal	576	+0.00000	[+0.00000, +0.00000]	14.2%	YES
no_mad_lognormal	576	+0.00000	[+0.00000, +0.00000]	9.9%	YES
weighted_arithmetic	576	+0.00027	[+0.00009, +0.00048]	42.2%	YES

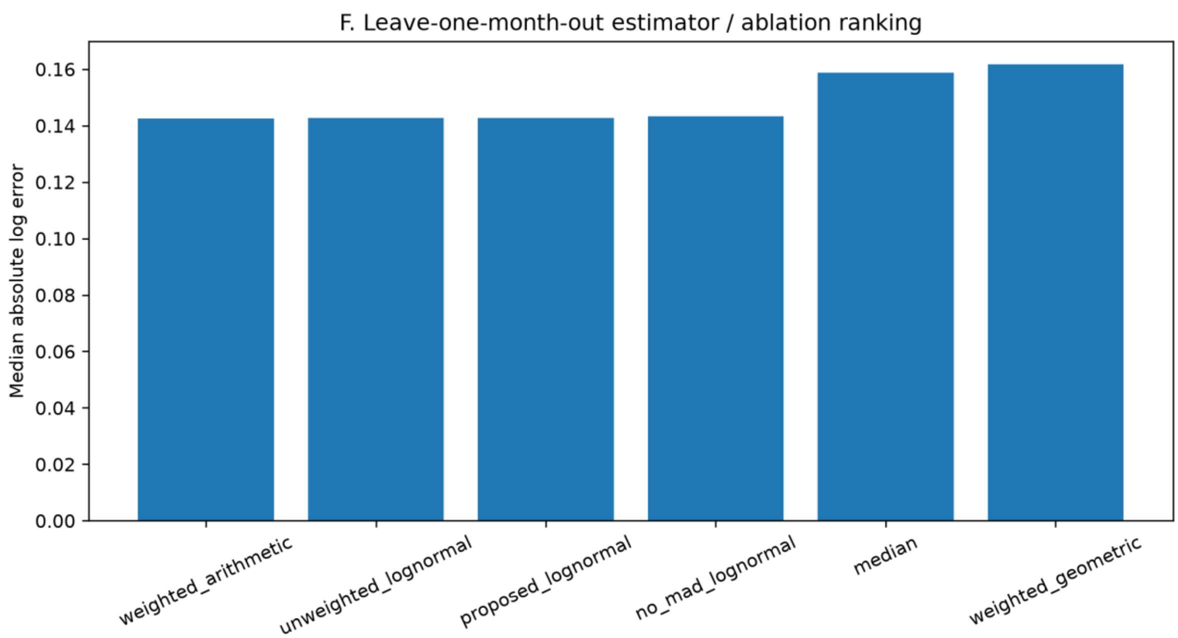

Figure S7. Leave-one-month-out temporal hold-out comparison. Lower median absolute log discrepancy indicates closer agreement between an annual estimate derived from the remaining months and the omitted-month radiance. This is a temporal representativeness diagnostic, not a forecast-skill test.

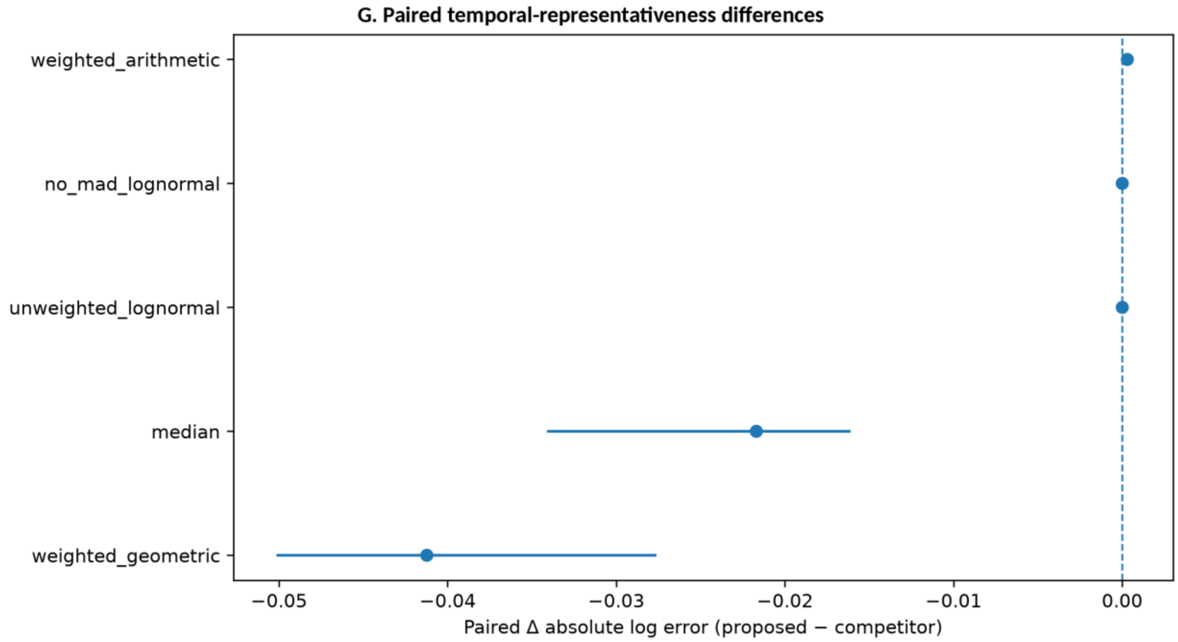

Figure S8. Paired difference in temporal hold-out absolute log discrepancy between the proposed estimator and each comparator after collapse to point-year cluster medians. Negative values favour the proposed method; bars are cluster-bootstrap 95% confidence intervals.

S5.4 Component ablations

Ablation	n	Median Δ	Median |Δ|	P90 |Δ|	Max |Δ|
FULL_proposed_lognormal	576	+0.000%	0.000%	0.000%	0.00%
NO_MAD_lognormal	576	+0.000%	0.000%	1.378%	68.31%
NO_QA_weights_unweighted_lognormal	576	+0.000%	0.000%	0.000%	0.38%
WEIGHTED_arithmetic	576	-0.188%	0.396%	1.818%	11.81%
ROBUST_median	576	-10.840%	10.840%	22.825%	49.81%
NO_logvariance_correction_geometric	576	-11.609%	11.609%	19.907%	40.96%

The lognormal variance correction is the dominant structural distinction from a geometric mean: removing it changes the annual estimate by 11.61% in median absolute terms. Replacing the full estimator by the robust median changes it by 10.84% in median absolute terms. Weighted arithmetic is much closer (0.40% median absolute difference). QA weighting has negligible influence in the present panel because nearly all eligible observations have q=1.0. MAD screening has little median influence but can be important for isolated point-years, with a maximum change of 68.31%.

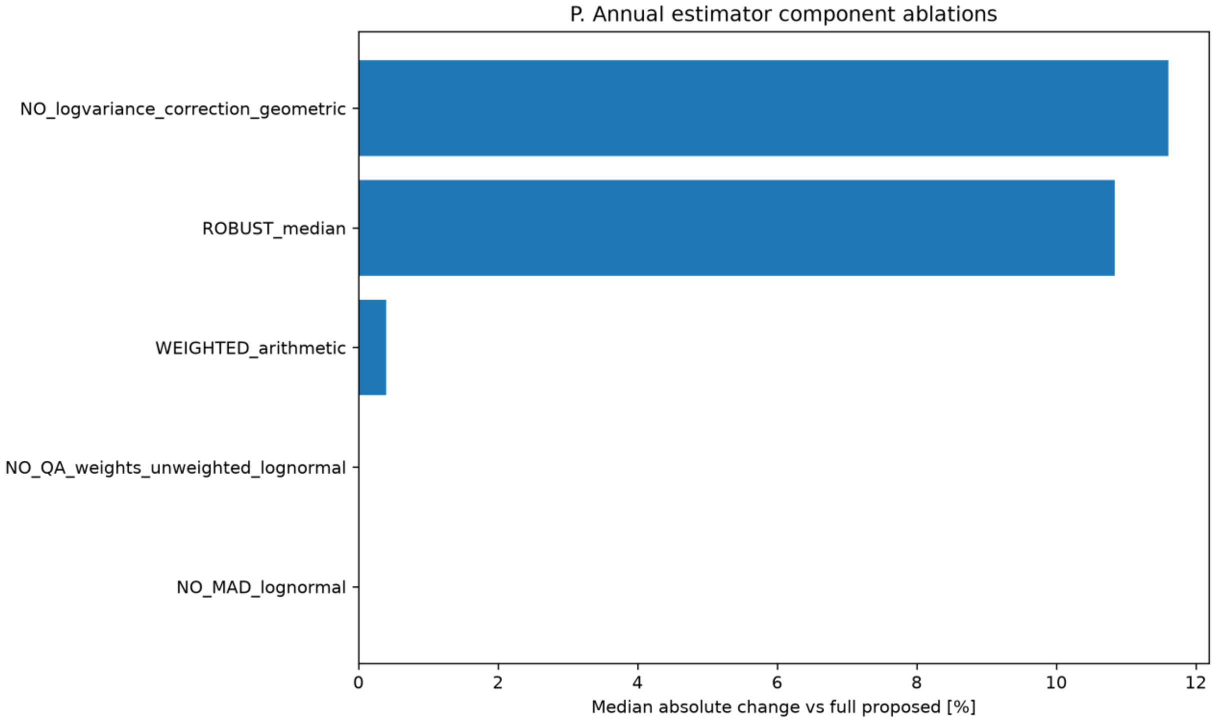

Figure S9. Median absolute change in annual radiance when individual components of the proposed estimator are removed or replaced. The log-variance correction is the principal structural difference from the geometric mean.

S5.5 Temporal-dependence-aware uncertainty

The median bootstrap/parametric interval-width ratio was 1.124× (mean 1.151×). The 90th percentile was 1.387×. Thus the analytical conditional interval is, on average, narrower than a dependence-aware moving-block bootstrap interval. This does not invalidate the point estimate, but it limits interpretation of ci95_low/ci95_high as a complete uncertainty envelope.

Uncertainty diagnostic	Result
Bootstrap valid replicates per point-year	500
Median parametric width	0.8449
Median bootstrap width	0.9708
Median width ratio	1.124×
P90 width ratio	1.387×
Empirical mean inside parametric interval	100.0%
Empirical mean inside bootstrap interval	100.0%

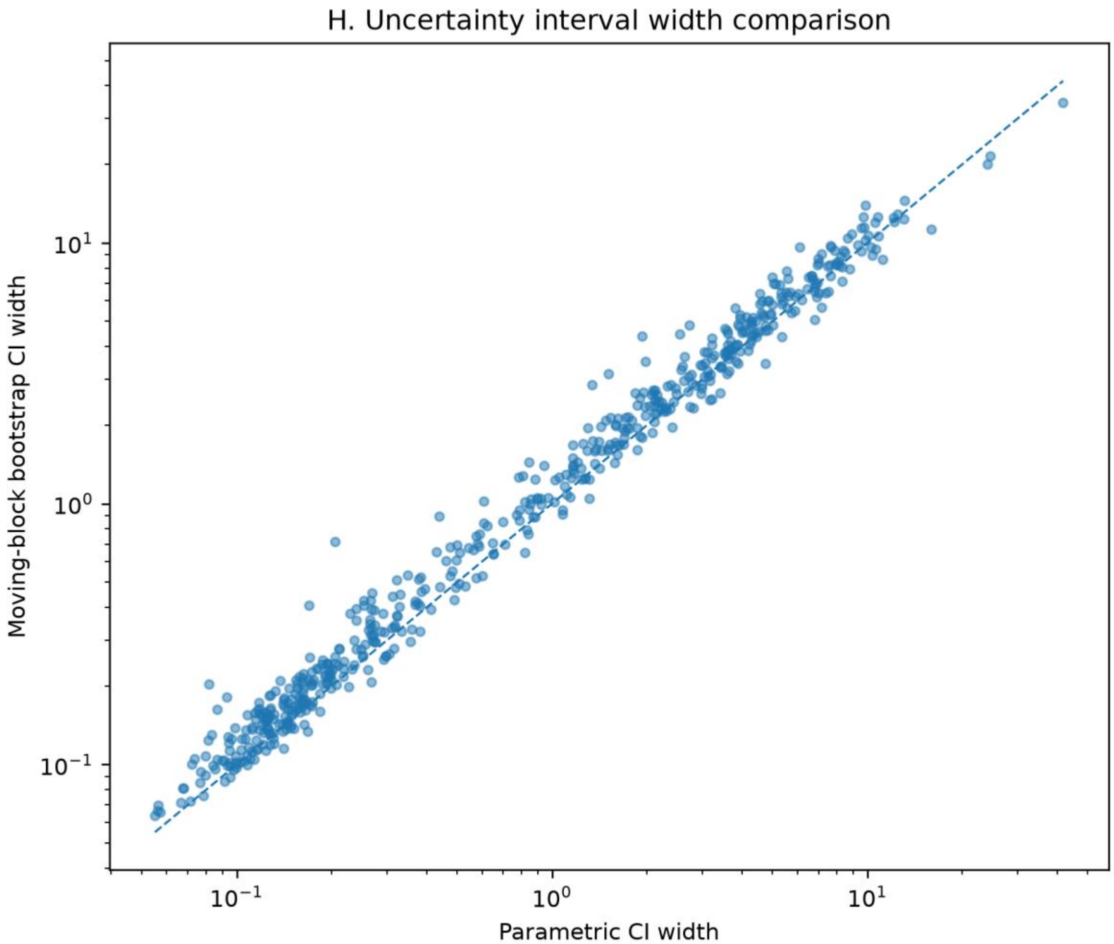

Figure S10. Conditional parametric 95% interval width versus moving-block bootstrap interval width. Values above the 1:1 line indicate inflation when temporal dependence is retained.

S5.6 QA reliability-weight evidence

Cloud confidence	Cloud-mask quality	n	Robust σ(log)	Fixed q	Empirical relative weight
0	2	10993	0.4654	1.00	0.935
0	3	47084	0.4500	1.00	1.000
1	3	13	0.4843	0.70	0.863

The global rank agreement between the fixed q values and empirical inverse-variance relative weights was Spearman ρ=0.866. In this panel, 99.976% of eligible observations were assigned q=1.0 and only 14 observations received q=0.7. The result therefore supports the ordering of the assigned QA weights, while the exact numerical difference between the weight levels remains only weakly constrained by this dataset.

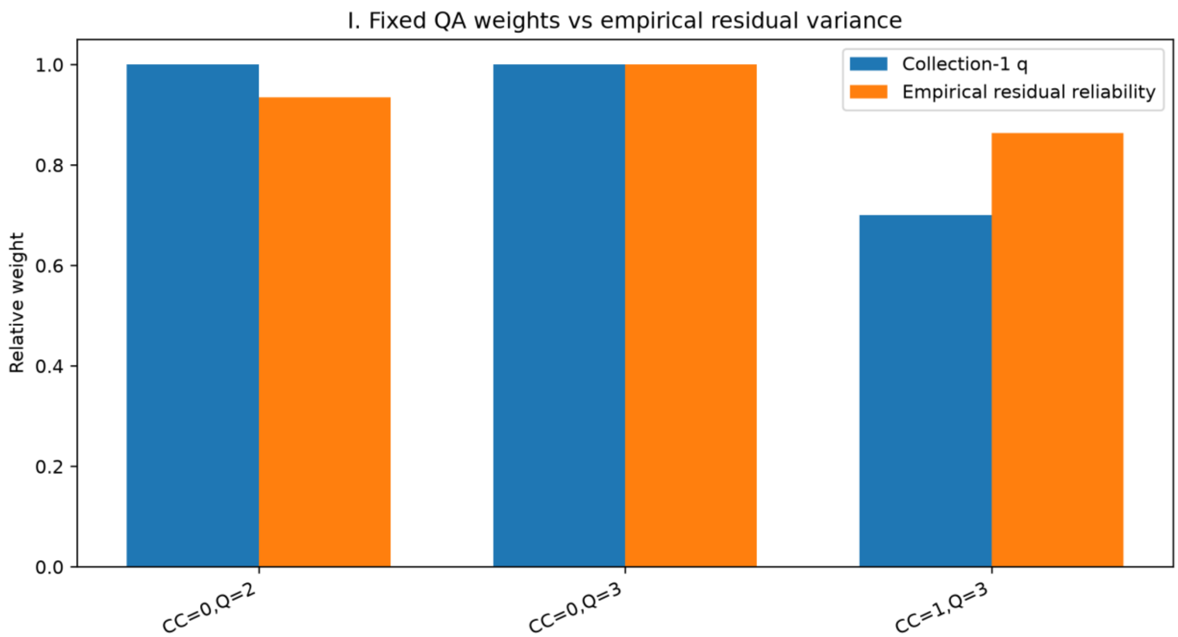

Figure S11. Fixed Collection-1 QA reliability weights compared with relative inverse residual-variance weights estimated from the validation panel. This is an ordering diagnostic, not a sensor error-covariance calibration.

S5.7 Parameter sensitivity

Scenario	n	Median Δ	Median |Δ|	P90 |Δ|	Max |Δ|
low_cloud_mask_quality_weight=0.7	576	+0.000%	0.000%	0.000%	0.00%
low_cloud_mask_quality_weight=0.9	576	+0.000%	0.000%	0.000%	0.00%
mad_multiplier=3.0	576	+0.000%	0.000%	1.546%	13.76%
min_radiance=0.05	576	+0.000%	0.000%	1.246%	15.85%
mad_multiplier=4.0	576	+0.000%	0.000%	0.540%	8.26%
probably_clear_weight=0.6	576	+0.000%	0.000%	0.000%	0.13%
min_radiance=0.2	576	+0.000%	0.000%	8.451%	47.09%
uncertainty_range_log=0.4	576	+0.000%	0.000%	0.000%	0.01%
uncertainty_range_log=0.2	576	+0.000%	0.000%	0.000%	0.01%
probably_clear_weight=0.8	576	+0.000%	0.000%	0.000%	0.13%
lunar_max=40.0	576	-0.623%	1.003%	2.664%	7.22%
lunar_max=20.0	576	+0.314%	1.019%	2.971%	11.57%

Sensitivity is moderate overall but not uniform. The lunar threshold shifts the estimate by about 1% in median absolute terms and up to 2.97% at P90. Raising the radiance floor from 0.10 to 0.20 nW cm^{-2} sr^{-1} has the largest P90 impact (8.45%) and a maximum impact of 47.09%, demonstrating that near-floor behaviour is a scientifically important parameter choice. Changing QA weights has negligible effect in this panel because the relevant low-reliability observations are rare.

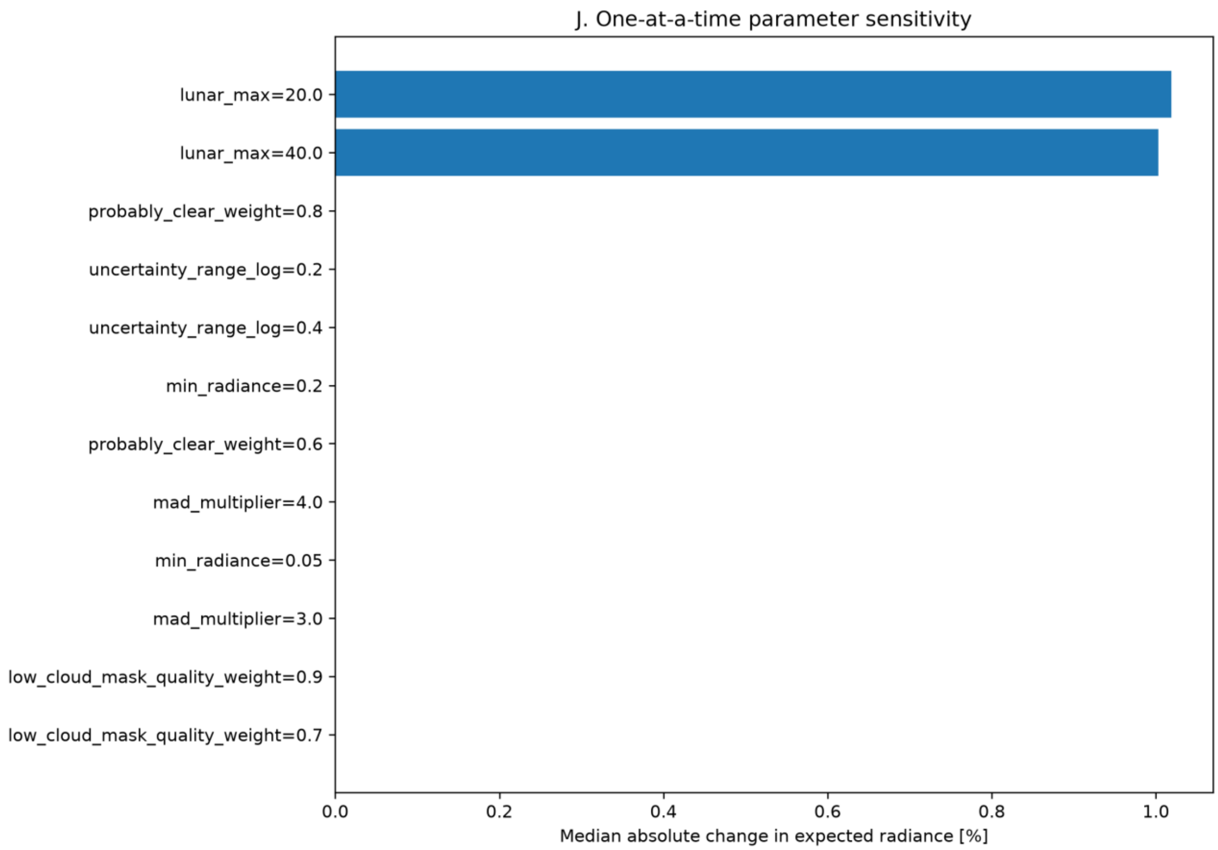

Figure S12. One-at-a-time sensitivity of annual expected radiance to plausible parameter changes. Larger changes identify parameters requiring explicit interpretation and version control.

S5.8 Effective temporal support and convergence

n_eff threshold	Subsample estimates retained	P90 absolute error vs full-year	Share within 5%
2	172,799	13.03%	62.8%
5	172,653	13.00%	62.9%
10	171,030	12.74%	63.3%
15	166,259	12.18%	64.3%
20	158,842	11.55%	65.8%
30	137,339	10.03%	69.6%
40	111,641	8.63%	74.1%
60	70,741	6.85%	81.1%
80	40,946	5.75%	86.2%
120	2,045	4.45%	92.6%

The first tested threshold satisfying the prespecified P90 absolute error ≤5% rule was n_eff=120, where P90 error was 4.45% and 92.6% of subsample estimates were within 5% of the full-year estimator. This does not mean that n_eff<120 is mathematically invalid. Rather, n_eff≥120 is an empirically supported high-stability interpretation tier for this panel.

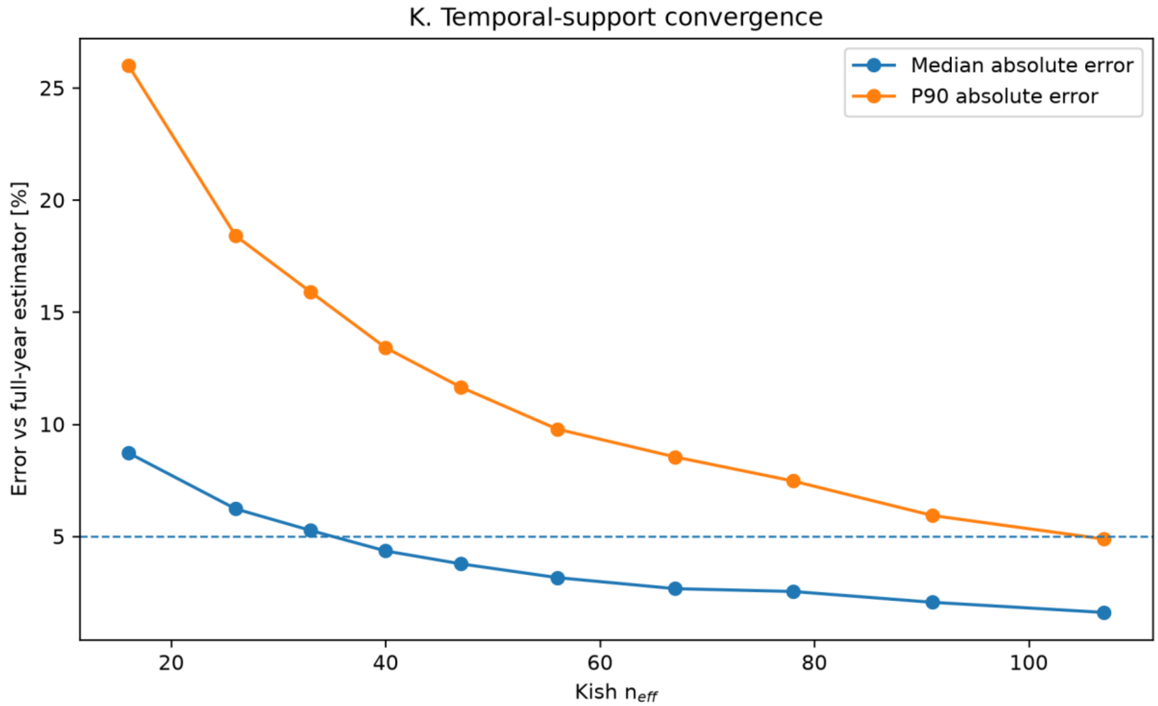

Figure S13. Error of month-block subsamples relative to the full-year estimator as a function of Kish effective sample size. The horizontal 5% line defines the validation stability criterion.

S5.9 External EOG cross-product consistency

Across 576 matched point-years, the EOG comparison yielded Spearman ρ=0.117, median difference=2.180 nW cm^{-2} sr^{-1}, median absolute difference=5.378 nW cm^{-2} sr^{-1}, RMSE=26.519 nW cm^{-2} sr^{-1} and median absolute log-ratio=1.566. Agreement is weak, showing that the two compositing chains are not interchangeable and that brightness-dependent residual structure remains substantial.

Site	n	Spearman rho	Median |log ratio|
Belo Horizonte	96	0.164	1.404
Brasilia	96	0.122	1.826
Manaus	96	0.436	1.568
Porto Alegre	96	0.051	1.504
Recife	96	-0.159	1.430
Sao Paulo	96	0.360	1.982

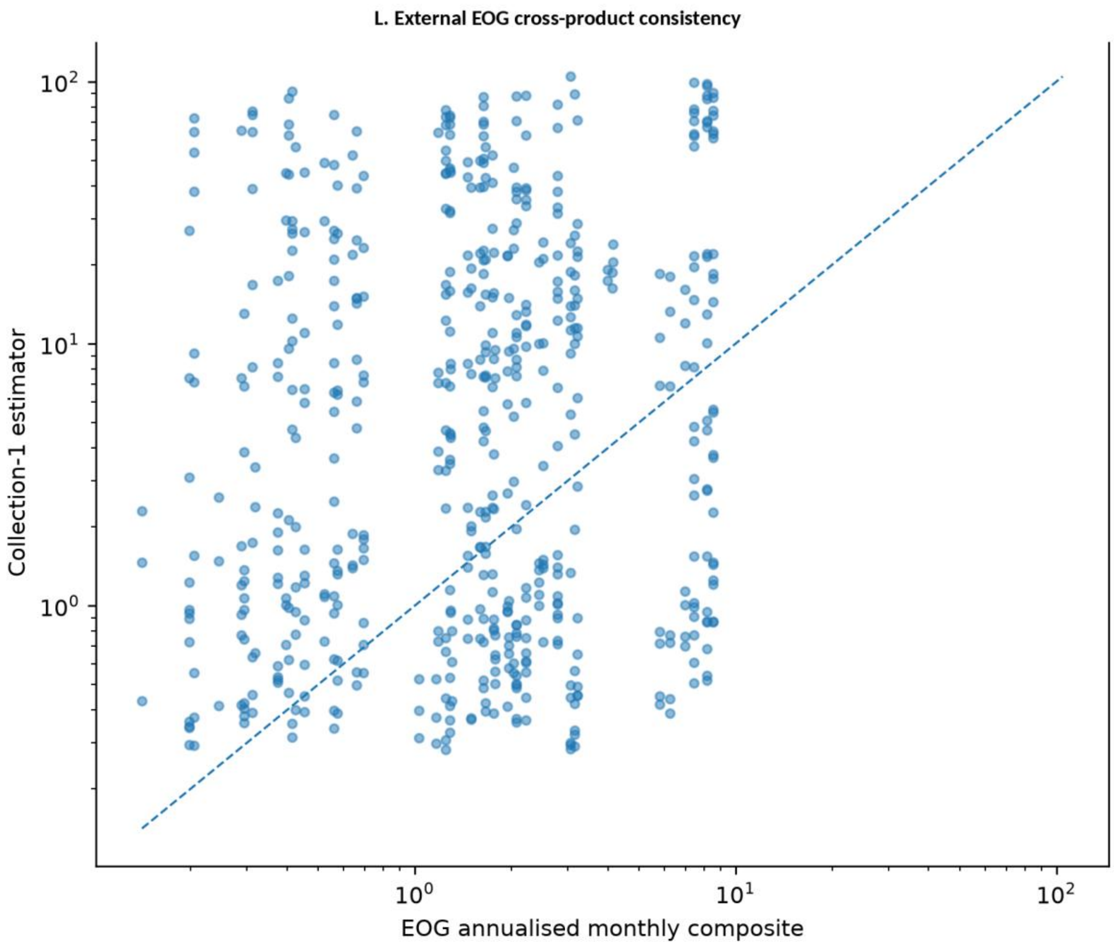

Figure S14. Collection 1 estimator versus an annualised EOG monthly VIIRS composite weighted by cloud-free coverage. The comparison quantifies agreement between two different VIIRS processing chains.

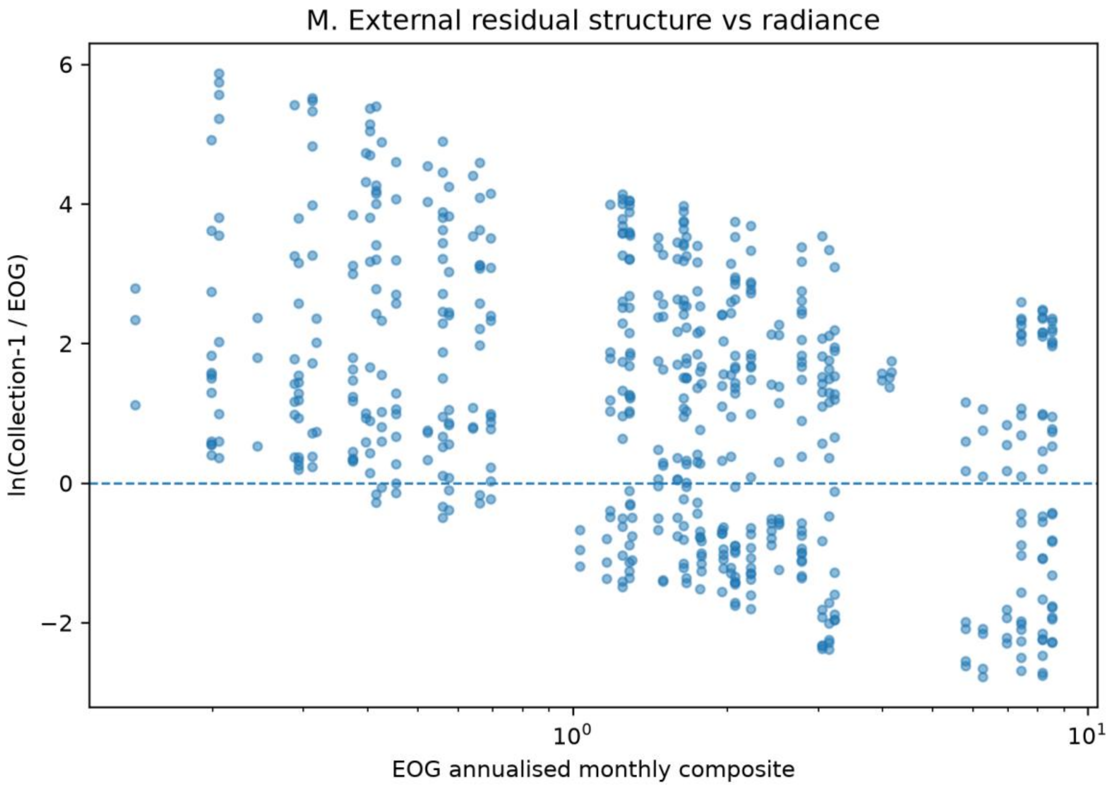

Figure S15. Log-ratio residual between Collection-1 and EOG versus EOG radiance. Structured residuals reveal brightness-dependent disagreement between the two compositing approaches.

S5.10 Geographical, temporal and brightness-regime robustness

Site	n	Median radiance	Median n_eff	Median |D_LN|	P90 |D_LN|
Belo Horizonte	96	3.923	126.5	0.360%	1.946%
Brasilia	96	5.989	106.0	0.658%	2.302%
Manaus	96	4.059	53.5	0.438%	1.345%
Porto Alegre	96	2.512	113.0	0.375%	3.410%
Recife	96	4.573	127.0	0.425%	1.655%
Sao Paulo	96	4.003	83.0	0.205%	0.941%

Year	n	Median radiance	Median n_eff	Median |D_LN|	P90 |D_LN|
2019	192	3.542	110.0	0.435%	1.867%
2021	192	4.054	107.0	0.372%	1.738%
2024	192	5.491	100.0	0.393%	1.546%

Median |D_LN| remains below 0.66% at every validation site and below 0.48% in every radiance stratum, indicating that the annual lognormal mean correction is not driven by a single city or brightness class. P90 discrepancies are larger in Porto Alegre (3.41%) and Brasília (2.30%) but remain small in absolute terms relative to the multi-order-of-magnitude radiance range.

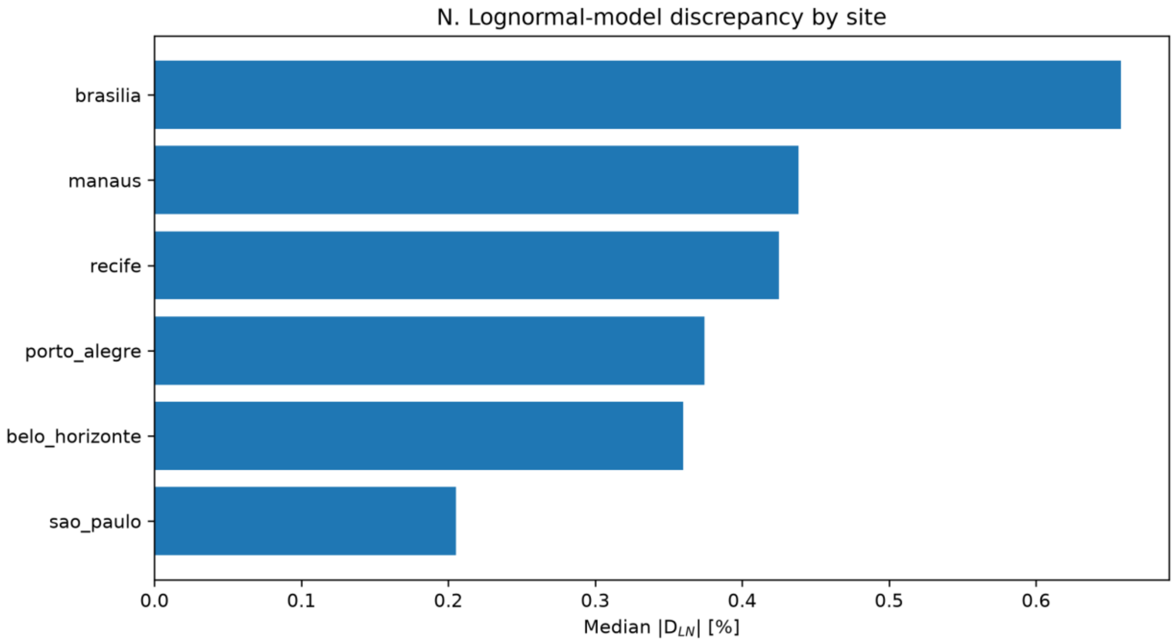

Figure S16. Median absolute lognormal-model discrepancy by validation site.

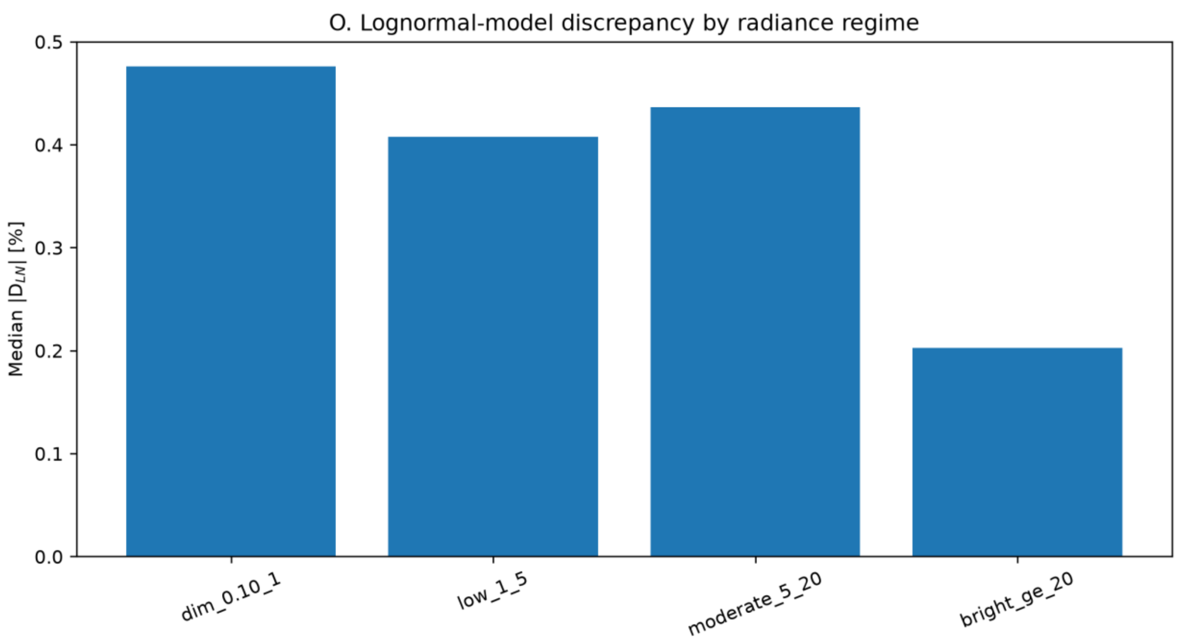

Figure S17. Median absolute lognormal-model discrepancy across near-floor to bright radiance regimes.

S5.11 Why lognormal is retained: information content

Weighted arithmetic and the lognormal expectation answer nearly the same annual-magnitude question in this panel; their median absolute difference is only 0.40%. The scientific reason for retaining the lognormal formulation is the additional distributional structure: the estimator exposes weighted log-location μw and within-year log variance s_v^2, and carries that dispersion into annual expected radiance through $\exp(s\_v^2/2)$.

Figure S18 makes the distinction explicit. Relative to weighted arithmetic, expected_radiance remains close to zero difference over most of the observed variance range. Relative to the weighted geometric level, however, the variance correction grows systematically with s_v^2. Thus the product preserves annual magnitude while additionally indicating how strongly within-year variability contributes to that magnitude.

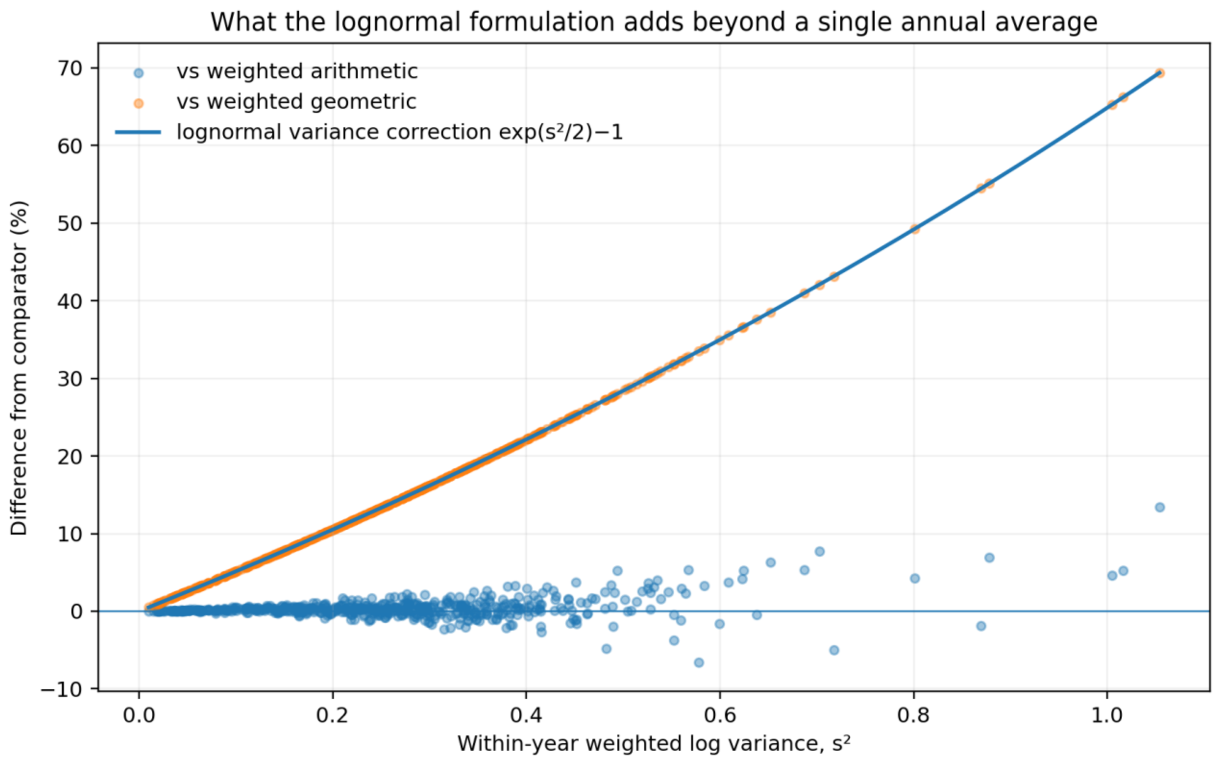

Figure S18. Information added by the lognormal formulation. Differences from the weighted arithmetic mean remain small for most point-years, whereas the difference from the weighted geometric level increases deterministically with within-year log variance through $\exp(s\_v^2/2)$. The figure therefore separates annual magnitude agreement from the additional information carried by within-year dispersion.

S6. Scientific interpretation

S6.1 What the lognormal formulation adds

- The lognormal formulation is a distribution-aware annual estimator. Across the 576 point-years, expected_radiance remains very close to the empirical weighted arithmetic expectation (median absolute difference 0.40%; P90 1.83%), so the model does not materially distort the annual radiance magnitude.
- Its added information is the explicit separation of weighted log-location μw and within-year log variance s_v^2. The annual expectation $L=R_0\exp(\mu w+s\_v^2/2)$ therefore records both the central radiance level and the contribution of multiplicative dispersion, while a single arithmetic mean collapses these components into one number. Median, P10 and P90 remain

distributed so that intermittent or non-lognormal profiles can be inspected without forcing the parametric interpretation.

- This distinction is substantive: removing the variance correction and reverting to the weighted geometric level changes annual radiance by 11.61% in median absolute terms. For interannual interpretation, the formulation also permits the exact decomposition $\Delta \ln(L) = \Delta \mu w + 0.5 \Delta s\_v^2$, separating a shift in central log-radiance from a change in within-year dispersion. In the 384 analysed interannual transitions, the dispersion term accounted for at least 10% of the absolute two-component decomposition in 52.9% of transitions and at least 25% in 23.4%.
- Effective temporal support matters strongly. Empirical stability improves continuously with n_eff, with n_eff=120 meeting the P90 ≤5% subsampling-error criterion in this panel.

S6.2 What is supported only with qualification

- The analytical conditional uncertainty interval is directionally useful but is narrower than the moving-block bootstrap interval on median (1.124× width ratio). It should not be marketed as a complete uncertainty budget.
- The fixed QA-weight ordering is consistent with the empirical variance ordering (Spearman ρ=0.866), but observations assigned reduced QA weights are too rare in this panel to strongly determine the exact numerical difference between the weight levels.
- MAD screening has little effect for the typical point-year but can have very large effects in isolated cases; therefore outlier_fraction should remain an exposed diagnostic.
- Parameter sensitivity is generally modest but the minimum-radiance floor and lunar threshold are scientifically material choices and should remain explicitly versioned.

S6.3 Scope of inference

- The experiments quantify the behaviour of the annual estimator, its temporal support and its distributional diagnostics across the tested VNP46A2 observations. No separate instrument measuring spectrally and temporally matched upward radiance was included in this validation dataset.
- The 192 fixed locations span six geographically distinct Brazilian domains and four radiance regimes. The geographical conclusions of this report therefore refer to the environmental and radiance conditions represented by these validation domains.

S7. References

Aitchison, J. & Brown, J.A.C. (1957). The Lognormal Distribution. Cambridge University Press.

Elvidge, C.D., Baugh, K., Zhizhin, M., Hsu, F.-C. & Ghosh, T. (2017). VIIRS night-time lights. International Journal of Remote Sensing, 38(21), 5860–5879. https://doi.org/10.1080/01431161.2017.1342050.

Elvidge, C.D., Zhizhin, M., Ghosh, T., Hsu, F.-C. & Taneja, J. (2021). Annual time series of global

VIIRS nighttime lights derived from monthly averages: 2012 to 2019. Remote Sensing, 13(5), 922. https://doi.org/10.3390/rs13050922.

Kish, L. (1965). Survey Sampling. John Wiley & Sons.

Levin, N. et al. (2020). Remote sensing of night lights: a review and an outlook for the future. Remote Sensing of Environment, 237, 111443. https://doi.org/10.1016/j.rse.2019.111443.

NASA VIIRS Land Science Investigator-led Processing System (2024a). Black Marble User Guide, Collection 2.0. NASA.

NASA VIIRS Land Science Investigator-led Processing System (2024b). VIIRS/NPP Gap-Filled Lunar BRDF-Adjusted Nighttime Lights Daily L3 Global 15 arc-second Linear Lat Lon Grid, Collection 2. https://doi.org/10.5067/VIIRS/VNP46A2.002.

Román, M.O. et al. (2018). NASA's Black Marble nighttime lights product suite. Remote Sensing of Environment, 210, 113–143. https://doi.org/10.1016/j.rse.2018.03.017.

Rousseeuw, P.J. & Croux, C. (1993). Alternatives to the median absolute deviation. Journal of the American Statistical Association, 88(424), 1273–1283. https://doi.org/10.1080/01621459.1993.10476408.

Small, C. (2021). Spatiotemporal characterization of VIIRS night light. Frontiers in Remote Sensing, 2, 775399. https://doi.org/10.3389/frsen.2021.775399.

Tan, X., Zhu, X., Chen, J. & Chen, R. (2021). Modeling the direction and magnitude of angular effects in nighttime light remote sensing. Remote Sensing of Environment, 269, 112834. https://doi.org/10.1016/j.rse.2021.112834.

Wang, Z., Román, M.O., Kalb, V.L., Miller, S.D., Zhang, J. & Shrestha, R.M. (2021). Quantifying uncertainties in nighttime light retrievals from Suomi-NPP and NOAA-20 VIIRS Day/Night Band data. Remote Sensing of Environment, 263, 112557. https://doi.org/10.1016/j.rse.2021.112557.

Wang, Z., Shrestha, R.M., Román, M.O. & Kalb, V.L. (2022). NASA's Black Marble multiangle nighttime lights temporal composites. IEEE Geoscience and Remote Sensing Letters, 19, 2505105. https://doi.org/10.1109/LGRS.2022.3176616.

Zheng, Q., Weng, Q., Zhou, Y. & Dong, B. (2022). Impact of temporal compositing on nighttime light data and its applications. Remote Sensing of Environment, 274, 113016. https://doi.org/10.1016/j.rse.2022.113016.

Appendix S-A. Full fixed validation-location registry

Coordinates below define the 192 native-support validation locations selected using the 2024 radiance strata and reused unchanged in 2019, 2021 and 2024.

Point ID	Site	Stratum	Stratum label	Latitude	Longitude	2024 reference radiance
belo_horizonte__0	Belo Horizonte	1	dim 0.10 1	-19.630435	-43.768166	0.9146
belo_horizonte__1	Belo Horizonte	1	dim 0.10 1	-19.949337	-43.687318	0.7366
belo_horizonte__2	Belo Horizonte	1	dim 0.10 1	-19.625943	-43.808591	0.8303
belo_horizonte__3	Belo Horizonte	1	dim 0.10 1	-19.729249	-43.610961	0.5465
belo_horizonte__4	Belo Horizonte	1	dim 0.10 1	-20.052643	-43.714268	0.5872
belo_horizonte__5	Belo Horizonte	1	dim 0.10 1	-19.711283	-43.732234	0.8889
belo_horizonte__6	Belo Horizonte	1	dim 0.10 1	-19.868488	-43.579520	0.6330
belo_horizonte__7	Belo Horizonte	1	dim 0.10 1	-19.769674	-43.597487	0.7883
belo_horizonte__10	Belo Horizonte	2	low 1 5	-19.751707	-43.781641	1.2498
belo_horizonte__11	Belo Horizonte	2	low 1 5	-20.025693	-43.795116	1.3385
belo_horizonte__12	Belo Horizonte	2	low 1 5	-20.106542	-44.060119	1.1765
belo_horizonte__13	Belo Horizonte	2	low 1 5	-19.621452	-44.069102	3.2263
belo_horizonte__14	Belo Horizonte	2	low 1 5	-19.881963	-43.628928	1.1929
belo_horizonte__15	Belo Horizonte	2	low 1 5	-20.070609	-44.028678	1.2190
belo_horizonte__8	Belo Horizonte	2	low 1 5	-20.039168	-43.889439	3.2697
belo_horizonte__9	Belo Horizonte	2	low 1 5	-19.823573	-43.750200	1.3625
belo_horizonte__16	Belo Horizonte	3	moderate 5 20	-20.048151	-44.248765	6.6649
belo_horizonte__17	Belo Horizonte	3	moderate 5 20	-19.625943	-43.956813	5.4703
belo_horizonte__18	Belo Horizonte	3	moderate 5 20	-19.994252	-44.208341	14.0871
belo_horizonte__19	Belo Horizonte	3	moderate 5 20	-19.616960	-43.880456	10.5040
belo_horizonte__20	Belo Horizonte	3	moderate 5 20	-19.863997	-44.131984	10.7429
belo_horizonte__21	Belo Horizonte	3	moderate 5 20	-20.030185	-44.172408	8.3793
belo_horizonte__22	Belo Horizonte	3	moderate 5 20	-19.693317	-43.956813	12.8409
belo_horizonte__23	Belo Horizonte	3	moderate 5 20	-19.877471	-44.087068	16.8369
belo_horizonte__24	Belo Horizonte	4	bright ge 20	-20.142474	-44.217324	23.9733
belo_horizonte__25	Belo Horizonte	4	bright ge 20	-19.751707	-44.087068	31.7356
belo_horizonte__26	Belo Horizonte	4	bright ge 20	-19.944845	-43.920880	65.0205
belo_horizonte__27	Belo Horizonte	4	bright ge 20	-20.003236	-43.929863	20.1386

Point ID	Site	Stratum	Stratum label	Latitude	Longitude	2024 reference radiance
belo_horizonte__28	Belo Horizonte	4	bright ge 20	-19.895438	-43.804099	31.6815
belo_horizonte__29	Belo Horizonte	4	bright ge 20	-19.823573	-43.983762	37.5158
belo_horizonte__30	Belo Horizonte	4	bright ge 20	-19.926879	-44.136476	43.4761
belo_horizonte__31	Belo Horizonte	4	bright ge 20	-19.926879	-43.920880	80.7209
brasilia__0	Brasilia	1	dim 0.10 1	-16.118022	-47.824060	0.9688
brasilia__1	Brasilia	1	dim 0.10 1	-15.561067	-48.228302	0.4809
brasilia__2	Brasilia	1	dim 0.10 1	-15.736238	-47.599481	0.7542
brasilia__3	Brasilia	1	dim 0.10 1	-15.475727	-48.093555	0.4188
brasilia__4	Brasilia	1	dim 0.10 1	-15.516151	-47.545582	0.6383
brasilia__5	Brasilia	1	dim 0.10 1	-16.019207	-47.738720	0.8523
brasilia__6	Brasilia	1	dim 0.10 1	-15.502676	-47.958807	0.4644
brasilia__7	Brasilia	1	dim 0.10 1	-16.032682	-47.657872	0.5197
brasilia__10	Brasilia	2	low 1 5	-16.037174	-47.895925	1.2516
brasilia__11	Brasilia	2	low 1 5	-15.727255	-47.725245	1.6929
brasilia__12	Brasilia	2	low 1 5	-16.104547	-47.886942	2.1301
brasilia__13	Brasilia	2	low 1 5	-15.668864	-48.120504	4.2718
brasilia__14	Brasilia	2	low 1 5	-15.655390	-47.594990	1.2668
brasilia__15	Brasilia	2	low 1 5	-15.897935	-47.702787	1.4188
brasilia__8	Brasilia	2	low 1 5	-16.077598	-47.828552	3.3823
brasilia__9	Brasilia	2	low 1 5	-15.596999	-47.922875	1.5107
brasilia__16	Brasilia	3	moderate 5 20	-15.987766	-48.071097	12.6390
brasilia__17	Brasilia	3	moderate 5 20	-15.821578	-47.837535	7.7409
brasilia__18	Brasilia	3	moderate 5 20	-15.956325	-48.133979	5.9442
brasilia__19	Brasilia	3	moderate 5 20	-15.902426	-48.098046	12.7433
brasilia__20	Brasilia	3	moderate 5 20	-15.462252	-47.590498	6.7719
brasilia__21	Brasilia	3	moderate 5 20	-15.951834	-48.084571	8.1435
brasilia__22	Brasilia	3	moderate 5 20	-15.965308	-48.012706	12.0963
brasilia__23	Brasilia	3	moderate 5 20	-15.794628	-47.815077	6.0069
brasilia__24	Brasilia	4	bright ge 20	-16.104547	-48.071097	20.0456
brasilia__25	Brasilia	4	bright ge 20	-15.862002	-48.053130	21.9329
brasilia__26	Brasilia	4	bright ge 20	-15.839544	-48.098046	64.6609
brasilia__27	Brasilia	4	bright ge 20	-16.109039	-48.084571	23.6459
brasilia__28	Brasilia	4	bright ge 20	-15.857511	-47.833043	41.9055

Point ID	Site	Stratum	Stratum label	Latitude	Longitude	2024 reference radiance
brasilia__29	Brasilia	4	bright ge 20	-15.785645	-48.017198	38.4661
brasilia__30	Brasilia	4	bright ge 20	-16.140480	-47.958807	47.3786
brasilia__31	Brasilia	4	bright ge 20	-15.686831	-47.846518	23.0577
manaus__0	Manaus	1	dim 0.10 1	-3.312538	-59.780636	0.4131
manaus__1	Manaus	1	dim 0.10 1	-3.272113	-59.574024	0.3844
manaus__2	Manaus	1	dim 0.10 1	-2.966686	-60.333100	0.4199
manaus__3	Manaus	1	dim 0.10 1	-3.222706	-59.645889	0.5769
manaus__4	Manaus	1	dim 0.10 1	-2.760074	-59.479701	0.4519
manaus__5	Manaus	1	dim 0.10 1	-2.836431	-59.542583	0.3704
manaus__6	Manaus	1	dim 0.10 1	-3.281097	-59.919875	0.7195
manaus__7	Manaus	1	dim 0.10 1	-2.957703	-60.265727	0.5185
manaus__10	Manaus	2	low 1 5	-2.899313	-60.068097	1.4814
manaus__11	Manaus	2	low 1 5	-2.867872	-60.090555	1.1506
manaus__12	Manaus	2	low 1 5	-2.993636	-60.153437	1.1071
manaus__13	Manaus	2	low 1 5	-2.679225	-59.677330	1.3522
manaus__14	Manaus	2	low 1 5	-3.240672	-60.104030	3.9038
manaus__15	Manaus	2	low 1 5	-3.096942	-59.735721	1.0861
manaus__8	Manaus	2	low 1 5	-3.047535	-59.870468	3.9226
manaus__9	Manaus	2	low 1 5	-2.953211	-59.955808	2.0262
manaus__16	Manaus	3	moderate 5 20	-3.007110	-59.901909	5.3241
manaus__17	Manaus	3	moderate 5 20	-3.047535	-59.910892	17.4413
manaus__18	Manaus	3	moderate 5 20	-2.966686	-59.982757	15.3995
manaus__19	Manaus	3	moderate 5 20	-3.123891	-59.915384	6.6354
manaus__20	Manaus	3	moderate 5 20	-3.200248	-60.144454	18.2281
manaus__21	Manaus	3	moderate 5 20	-3.096942	-59.964791	17.5924
manaus__22	Manaus	3	moderate 5 20	-2.998127	-60.086064	6.8404
manaus__23	Manaus	3	moderate 5 20	-2.944228	-60.036656	7.5655
manaus__24	Manaus	4	bright ge 20	-3.074484	-60.018690	62.0168
manaus__25	Manaus	4	bright ge 20	-3.137366	-59.964791	48.2347
manaus__26	Manaus	4	bright ge 20	-3.114908	-60.009707	84.2737
manaus__27	Manaus	4	bright ge 20	-3.083467	-59.951316	46.8583
manaus__28	Manaus	4	bright ge 20	-3.083467	-59.883943	37.1280
manaus__29	Manaus	4	bright ge 20	-3.061009	-60.000724	66.9464

Point ID	Site	Stratum	Stratum label	Latitude	Longitude	2024 reference radiance
manaus__30	Manaus	4	bright ge 20	-3.029568	-60.000724	67.4919
manaus__31	Manaus	4	bright ge 20	-3.105925	-59.991740	80.5648
porto_alegre__0	Porto Alegre	1	dim 0.10 1	-30.428184	-51.507153	0.3717
porto_alegre__1	Porto Alegre	1	dim 0.10 1	-30.217080	-51.601476	0.3490
porto_alegre__2	Porto Alegre	1	dim 0.10 1	-30.059875	-51.498169	0.7727
porto_alegre__3	Porto Alegre	1	dim 0.10 1	-30.378777	-50.730110	0.3436
porto_alegre__4	Porto Alegre	1	dim 0.10 1	-30.023943	-50.873840	0.6306
porto_alegre__5	Porto Alegre	1	dim 0.10 1	-30.019451	-50.779517	0.4647
porto_alegre__6	Porto Alegre	1	dim 0.10 1	-30.392252	-51.444271	0.4085
porto_alegre__7	Porto Alegre	1	dim 0.10 1	-30.244030	-51.170284	0.5825
porto_alegre__10	Porto Alegre	2	low 1 5	-29.565802	-50.828925	1.1972
porto_alegre__11	Porto Alegre	2	low 1 5	-29.826313	-50.685194	1.3234
porto_alegre__12	Porto Alegre	2	low 1 5	-30.149707	-51.031046	2.3439
porto_alegre__13	Porto Alegre	2	low 1 5	-29.817330	-50.689686	1.6705
porto_alegre__14	Porto Alegre	2	low 1 5	-29.552327	-51.255624	2.4641
porto_alegre__15	Porto Alegre	2	low 1 5	-29.655633	-51.417321	1.1808
porto_alegre__8	Porto Alegre	2	low 1 5	-29.781397	-51.296049	2.1950
porto_alegre__9	Porto Alegre	2	low 1 5	-29.727499	-51.448762	1.0058
porto_alegre__16	Porto Alegre	3	moderate 5 20	-30.194622	-51.129860	9.8330
porto_alegre__17	Porto Alegre	3	moderate 5 20	-30.113774	-51.381388	5.4400
porto_alegre__18	Porto Alegre	3	moderate 5 20	-29.574785	-51.174776	5.4373
porto_alegre__19	Porto Alegre	3	moderate 5 20	-30.095808	-51.345456	16.1737
porto_alegre__20	Porto Alegre	3	moderate 5 20	-29.934111	-51.201725	12.8610
porto_alegre__21	Porto Alegre	3	moderate 5 20	-30.073350	-51.089436	14.4194
porto_alegre__22	Porto Alegre	3	moderate 5 20	-29.916145	-51.228675	10.1159
porto_alegre__23	Porto Alegre	3	moderate 5 20	-30.068858	-51.035537	10.9336
porto_alegre__24	Porto Alegre	4	bright ge 20	-30.131740	-51.309523	54.5124
porto_alegre__25	Porto Alegre	4	bright ge 20	-29.785889	-51.147826	50.7214
porto_alegre__26	Porto Alegre	4	bright ge 20	-30.158690	-51.161301	26.4826
porto_alegre__27	Porto Alegre	4	bright ge 20	-30.109283	-51.363422	21.3876
porto_alegre__28	Porto Alegre	4	bright ge 20	-29.907162	-51.062487	41.3358
porto_alegre__29	Porto Alegre	4	bright ge 20	-29.916145	-50.918756	20.2311
porto_alegre__30	Porto Alegre	4	bright ge 20	-29.651142	-51.165793	26.6574

Point ID	Site	Stratum	Stratum label	Latitude	Longitude	2024 reference radiance
porto_alegre__31	Porto Alegre	4	bright ge 20	-29.925128	-50.995113	50.6919
recife__0	Recife	1	dim 0.10 1	-7.844538	-34.704165	0.4602
recife__1	Recife	1	dim 0.10 1	-8.073609	-34.650266	0.4431
recife__2	Recife	1	dim 0.10 1	-8.100558	-34.740098	0.7133
recife__3	Recife	1	dim 0.10 1	-8.419460	-34.659249	0.3883
recife__4	Recife	1	dim 0.10 1	-7.840047	-35.045525	0.9211
recife__5	Recife	1	dim 0.10 1	-7.822080	-35.153323	0.9673
recife__6	Recife	1	dim 0.10 1	-7.884962	-34.686199	0.4747
recife__7	Recife	1	dim 0.10 1	-7.822080	-35.081458	0.8190
recife__10	Recife	2	low 1 5	-8.325137	-35.247646	1.4271
recife__11	Recife	2	low 1 5	-8.365561	-35.171289	1.2679
recife__12	Recife	2	low 1 5	-7.866996	-35.045525	1.1382
recife__13	Recife	2	low 1 5	-7.956828	-35.198239	1.0779
recife__14	Recife	2	low 1 5	-8.410477	-34.942219	1.7625
recife__15	Recife	2	low 1 5	-7.902929	-34.973660	2.9651
recife__8	Recife	2	low 1 5	-7.817589	-34.865862	4.2048
recife__9	Recife	2	low 1 5	-8.078100	-35.027559	4.0652
recife__16	Recife	3	moderate 5 20	-8.347595	-34.964677	15.6228
recife__17	Recife	3	moderate 5 20	-7.943353	-35.014084	9.5028
recife__18	Recife	3	moderate 5 20	-8.037676	-35.094932	6.0469
recife__19	Recife	3	moderate 5 20	-8.105050	-35.045525	8.3947
recife__20	Recife	3	moderate 5 20	-8.334120	-35.005101	9.0439
recife__21	Recife	3	moderate 5 20	-7.947844	-34.919761	8.8006
recife__22	Recife	3	moderate 5 20	-7.938861	-35.000609	17.9076
recife__23	Recife	3	moderate 5 20	-8.114033	-34.879337	8.2741
recife__24	Recife	4	bright ge 20	-7.952336	-34.834421	21.4682
recife__25	Recife	4	bright ge 20	-8.100558	-34.928744	87.3783
recife__26	Recife	4	bright ge 20	-8.078100	-34.978151	62.3795
recife__27	Recife	4	bright ge 20	-8.397002	-35.063491	55.2717
recife__28	Recife	4	bright ge 20	-7.754707	-34.829929	26.7980
recife__29	Recife	4	bright ge 20	-8.019710	-34.955693	43.2687
recife__30	Recife	4	bright ge 20	-8.136491	-34.955693	61.8042
recife__31	Recife	4	bright ge 20	-7.983777	-34.915269	45.5933

Point ID	Site	Stratum	Stratum label	Latitude	Longitude	2024 reference radiance
sao_paulo__0	Sao Paulo	1	dim 0.10 1	-23.335985	-47.020068	0.9257
sao_paulo__1	Sao Paulo	1	dim 0.10 1	-23.318019	-47.069475	0.9880
sao_paulo__2	Sao Paulo	1	dim 0.10 1	-23.762685	-46.171160	0.7046
sao_paulo__3	Sao Paulo	1	dim 0.10 1	-23.996247	-47.047017	0.6110
sao_paulo__4	Sao Paulo	1	dim 0.10 1	-23.901924	-46.876337	0.9827
sao_paulo__5	Sao Paulo	1	dim 0.10 1	-24.000739	-46.723624	0.6074
sao_paulo__6	Sao Paulo	1	dim 0.10 1	-23.861500	-47.029051	0.6878
sao_paulo__7	Sao Paulo	1	dim 0.10 1	-23.942348	-46.894304	0.8306
sao_paulo__10	Sao Paulo	2	low 1 5	-23.888449	-46.341840	3.1847
sao_paulo__11	Sao Paulo	2	low 1 5	-23.282086	-46.849388	3.4152
sao_paulo__12	Sao Paulo	2	low 1 5	-24.041163	-46.391247	2.1374
sao_paulo__13	Sao Paulo	2	low 1 5	-23.273103	-46.966169	1.2928
sao_paulo__14	Sao Paulo	2	low 1 5	-23.924382	-46.710149	1.4568
sao_paulo__15	Sao Paulo	2	low 1 5	-23.223696	-46.225059	1.1762
sao_paulo__8	Sao Paulo	2	low 1 5	-23.367426	-46.503536	1.9812
sao_paulo__9	Sao Paulo	2	low 1 5	-24.014213	-46.328365	2.8301
sao_paulo__16	Sao Paulo	3	moderate 5 20	-23.542598	-47.141340	11.2896
sao_paulo__17	Sao Paulo	3	moderate 5 20	-23.434800	-46.835913	13.1986
sao_paulo__18	Sao Paulo	3	moderate 5 20	-23.627938	-46.283449	5.3743
sao_paulo__19	Sao Paulo	3	moderate 5 20	-23.587514	-47.033542	7.2605
sao_paulo__20	Sao Paulo	3	moderate 5 20	-23.857008	-46.714641	16.1772
sao_paulo__21	Sao Paulo	3	moderate 5 20	-23.812092	-46.543961	5.4538
sao_paulo__22	Sao Paulo	3	moderate 5 20	-23.627938	-47.020068	14.8794
sao_paulo__23	Sao Paulo	3	moderate 5 20	-23.789635	-46.534978	16.4098
sao_paulo__24	Sao Paulo	4	bright ge 20	-23.717769	-46.566419	86.9142
sao_paulo__25	Sao Paulo	4	bright ge 20	-23.412342	-46.305907	22.1996
sao_paulo__26	Sao Paulo	4	bright ge 20	-23.547089	-46.719132	65.0618
sao_paulo__27	Sao Paulo	4	bright ge 20	-23.551581	-46.314890	56.0939
sao_paulo__28	Sao Paulo	4	bright ge 20	-23.214713	-46.876337	76.7102
sao_paulo__29	Sao Paulo	4	bright ge 20	-23.547089	-46.548452	88.0002
sao_paulo__30	Sao Paulo	4	bright ge 20	-23.475224	-46.624809	63.2480
sao_paulo__31	Sao Paulo	4	bright ge 20	-23.627938	-46.768539	72.6146